Text and references accompanying Nevada Bureau of Mines and Geology Map 186

Geologic Map of the Humboldt Peak Quadrangle, Elko County, Nevada

by

Allen J. McGrew

University of Dayton

2018

ABSTRACT

Located in central Elko County, Nevada, the Humboldt Peak quadrangle exposes the central and highest part of the East Humboldt Range (EHR). It is flanked to the east by Clover Valley and a northerly trending line of hills. The central East Humboldt Range probably represents the structurally deepest part of the Ruby Mountains-East Humboldt Range metamorphic core complex. The high-grade core of the EHR consists of migmatitic upper amphibolite facies rocks that achieved peak P-T conditions during Late Cretaceous metamorphism up to 8 kb and 775°C. The deepest structural levels, exposed in Lizzies Basin in the west-central part of the quadrangle, form a migmatite complex with >67% leucogranitic rock. In the northwest part of the quadrangle, this migmatite complex is overlain in the cirque wall above Winchell Lake by a southward-closing, kilometer-scale recumbent fold known as the Winchell Lake fold-nappe (WLN). The WLN folds a sequence of intensely metamorphosed, migmatized and profoundly attenuated Neoproterozoic to Mississippian metasedimentary rocks. Farther north in the adjacent Welcome quadrangle the WLN is cored by Nevada's oldest rocks—Neoarchean to Early Paleoproterozoic orthogneiss and paragneiss that were thrust over the Neoproterozoic to Mississippian metasedimentary sequence before peak metamorphism and WLN-related folding. Overprinting this assemblage at higher structural levels is a WNW-directed, kilometer-scale mylonitic shear zone that diachronously exhumed this high-grade terrain during extensional tectonism bracketed between late Eocene and Miocene. Together, the mylonitic shear zone and the detachment fault that forms its roof probably accommodated much more than 15 km of extensional displacement. Cutting through the metamorphic core along the steep, eastern face of the East Humboldt Range is a younger, post-Miocene normal fault that remained active into the Quaternary. In the northern part of the quadrangle this normal fault uplifts and juxtaposes the high-grade core against moderately east-dipping Middle Miocene volcanic and hypabyssal intrusive rocks (rhyolitic quartz porphyry). A single exposure of flat-lying vitric tuff, also of Miocene age, lies to the east of the east-dipping rhyolite-bearing sequence, but it is unclear at present whether the flat-lying strata are faulted down against the rhyolitic rocks or overlie them in angular unconformity. The line of hills in the northeastern part of the quadrangle consists of Paleozoic sedimentary rock that probably represents the down-faulted "cover" of the metamorphic core complex. Finally, the late Quaternary basin fill to the east of this line of hills was faulted down against the Paleozoic sedimentary rocks along the Clover Valley fault, which strikes northward through the adjacent Welcome quadrangle toward the town of Wells where it may correlate with the fault that produced the M_w 6.0 Wells earthquake in 2008.

INTRODUCTION

The western part of the Humboldt Peak 7.5' quadrangle exposes the central and highest part of the East Humboldt Range (EHR), whereas the eastern part of the quadrangle is framed by Clover Valley, a basin filled with Cenozoic sedimentary, volcanic, and volcaniclastic rock, and by a north-trending line of hills underlain by Paleozoic bedrock (fig. 1; map plate). The earliest systematic reports on the geology of the EHR date from the 40th Parallel Survey led by Clarence King (1878), and it was later the focus of early studies on Basin-and-Range structure and geomorphology (Sharp, 1939, 1940). Prior to this study, the general geology of the EHR was mapped by Snelson (1957), and parts of the Humboldt Peak and Welcome quadrangles were mapped by Lush (1982) at 1:24,000 scale. The EHR along with the Ruby Mountains to the south and the Wood Hills to the east, have gained widespread attention as a classic example of a Cordilleran metamorphic core complex (Howard, 1980; Snoke, 1980; Snoke and Miller, 1988; Snoke et al., 1990; Snoke et al., 1997; McGrew et al., 2000; Sullivan and Snoke, 2007).

Recently, the EHR has also attracted attention due to seismic activity in the area. The hills on the east side of the

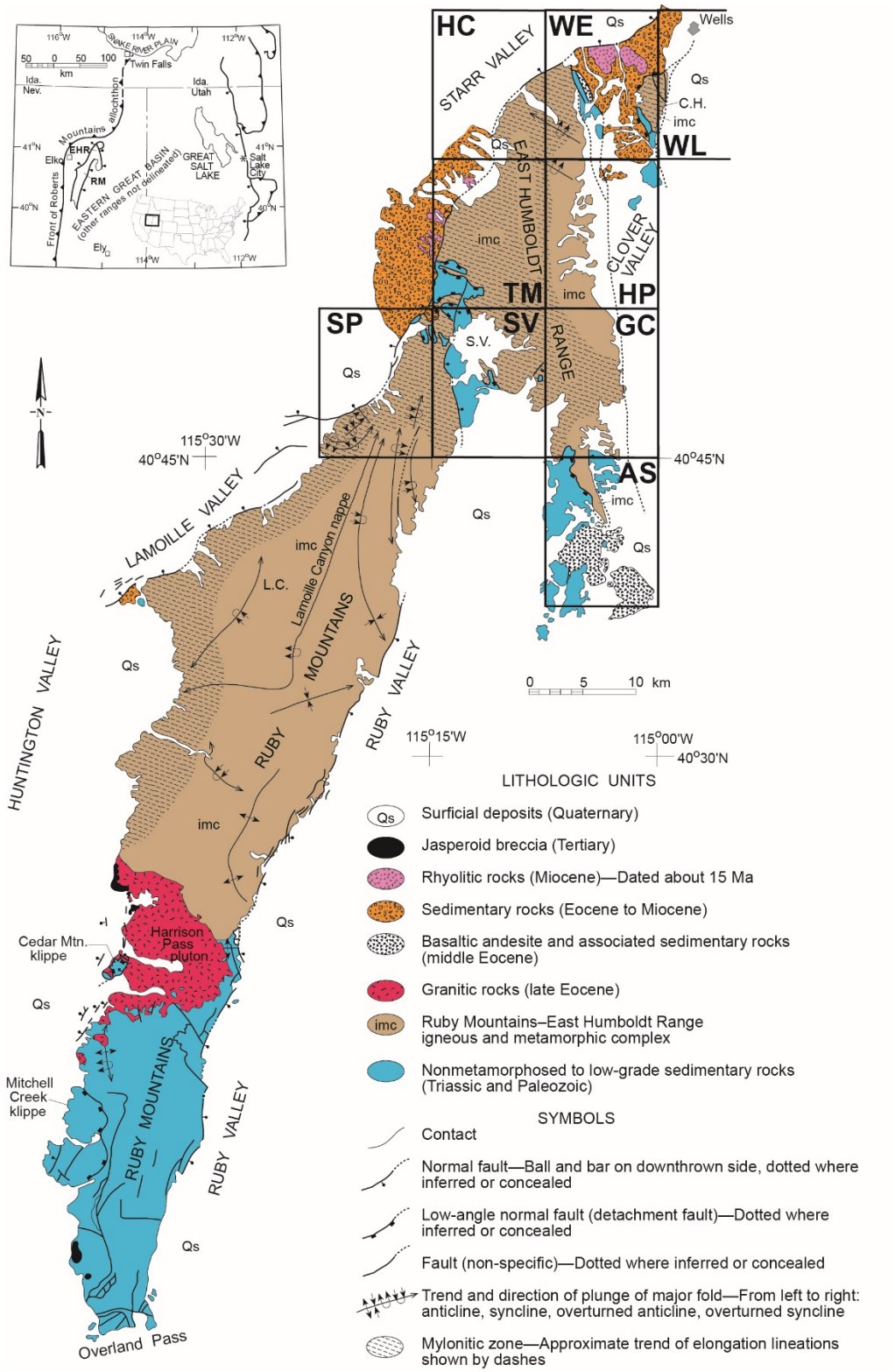

Figure 1. Generalized geologic map showing the location of the Humboldt Peak 7.5' quadrangle relative to other 7.5' quadrangles in the East Humboldt Range and northern Ruby Mountains. Inset shows map area in relation to other major tectonic elements of the western U.S. cordillera, including the Sevier fold-and-thrust belt and the leading edge of the Roberts Mountains allochthon. The names of 7.5' quadrangles are abbreviated as follows: Herder Creek (HC), Welcome (WE), Wells (WL), Tent Mountain (TM), Humboldt Peak (HP), Soldier Peak (SP), Secret Valley (SV), Gordon Creek (GC), and Arizona Springs (AS). Other abbreviations are: C.H. – Clover Hill, S.V. – Secret Valley, and L.C. – Lamoille Canyon. Modified from Snoke et al. (1997).

Humboldt Peak quadrangle are delineated by a normal fault that traces northward through the adjacent Welcome quadrangle along the base of Clover Hill toward the town of Wells, Nevada. Henry and Colgan (2011) suggested that this fault may correlate with the Wells earthquake fault—a blind normal fault underlying Town Creek Flat basin to the north of Wells and unrecognized until it produced the 6.0 magnitude (M_w) Wells earthquake on February 21, 2008 (dePolo and LaPointe, 2011; Thorman and Brooks, 2011).

With a ridgeline cresting above 3000 m for most of its length, the EHR is high enough that it supported widespread alpine glaciation during the Pleistocene, producing some of its most noteworthy physiographic landmarks. The highest peaks in the Humboldt Peak quadrangle are 11,306 ft (3446 m) Hole-in-the-Mountain Peak in the west-central part of the map and 11,020 ft (3359 m) Humboldt Peak in the southwestern part of the quadrangle. In the shadows of the precipitous ridge line, a series of deeply incised cirque basins commonly host cirque lakes, such as Winchell Lake, Lizzies Basin, and Steele Lake on the east side of the range, and Boulder Lake on the west (fig. 2a). The crest of the range through much of the Humboldt Peak quadrangle consists of sharp arêtes, the most spectacular of which forms the cirque wall west of Lizzies Basin and south of Hole-in-the-Mountain Peak. Near the crest of the Lizzies Basin arête an enclave of marble surrounded by more resistant granitoid rocks has eroded through the ridge line to create the distinctive landmark known as the Hole-in-the-Mountain (fig. 2b). Southern Clover Valley, just southeast of the Humboldt Peak quadrangle, hosted Pleistocene pluvial Lake Clover, and still today it hosts an ephemeral playa known as Snow Water Lake (Reheis et al., 2002; Munroe and Laabs, 2011, 2013). The Pleistocene history of the East Humboldt Range has been described by Sharp (1938), Wayne (1984), Osborn and Bevis (2001), and Munroe and Laabs (2011).

As outlined below, the Humboldt Peak quadrangle exposes a dissected natural cross section representing structural levels ranging from deep-crustal gneissic rocks to upper crustal Paleozoic sedimentary rocks and Cenozoic volcanic and sedimentary strata that are at least partly syntectonic with the uplift of the range. As such, this map area exposes critical relationships for reconstructing the history and architecture of the crust of the northeastern Great Basin. The central East Humboldt Range is accessible only by 4-wheel-drive trail, leading to a lack of coverage in field trip guidebooks, but some large framework elements of the geology can be viewed from Highway 93 (e.g., Snoke et al., 1997).

STRUCTURAL ARCHITECTURE

The EHR forms a north-trending horst block bounded on both the east and the west by major normal fault systems (Sharp, 1939; 1940). Foliations in the Humboldt Peak quadrangle dip variably northeastward along the east flank of the range and gently westward along the west side of the range, thus defining a gentle, north-trending arch with an axis approximately coincident with the range crest (map plate). The steep eastern flank of the range exposes a natural cross section through migmatitic upper amphibolite-facies rocks representing middle to deep-crustal levels, whereas the western flank of the range forms a dip-slope on the gently west-dipping Ruby Mountains-East Humboldt Range (RM-EHR) mylonitic shear zone (fig. 1; map plate) (Hurlow, 1987). From north-to-south, the range is broadly arched with the deepest structural levels in the center of the range in the vicinity of Lizzies Basin in the Humboldt Peak quadrangle (map plate).

The rocks of Lizzies Basin (henceforward referred to as the Lizzies Basin gneiss complex) dip gently northward toward Winchell Lake in the northwest part of the quadrangle where they are tectonically overlain by a large, southward-closing recumbent isoclinal fold (map plate, cross section A–A'). This fold, which is most spectacularly exposed in the cirque wall above Winchell Lake, is known as the Winchell Lake fold-nappe (WLN) (fig. 2c). The WLN is separated from the underlying Lizzies Basin gneiss complex by a low-angle tectonic contact inferred to represent the basal tectonic slide of the fold-nappe (map plate). This tectonic contact can be traced northeastward from an elevation of approximately 10,200 ft (3110 m) on the ridgeline due west of Winchell Lake to an elevation of approximately 8800 ft (2680 m) at the north edge of the quadrangle.

The Lizzies Basin gneiss complex consists of inferred lower Paleozoic metasedimentary rocks (mostly marble) overlying a thick sequence of paragneiss, quartzite, pelitic schist and subordinate marble that is here correlated with the Neoproterozoic to Lower Cambrian McCoy Creek Group and Prospect Mountain Quartzite (Misch and Hazzard, 1962; Miller, 1983). At the deepest structural levels on the east flank of the range, wholesale migmatization (67–90% leucogranite) commonly obliterates all vestiges of original stratigraphic relationships (fig. 2d; map plate). Intruding the Lizzies Basin gneiss complex is a thick hornblende biotite quartz diorite sheet that has been dated at 40 ± 3 Ma (ID-TIMS, U-Pb zircon lower intercept age; sample RM19 labeled "A" in a triangular box on the map plate) (Wright and Snoke, 1993). This quartz diorite sheet extends into the adjacent Welcome quadrangle where its northernmost exposures beneath Chimney Rock intrude into the lower limb of the WLN, thus cutting the basal tectonic slide of the fold-nappe and implying that emplacement of the WLN had to predate 40 Ma (McGrew and Snoke, 2015).

Though the WLN in the Humboldt Peak quadrangle primarily exposes high-grade metamorphosed Paleozoic strata, the northwestern part of the quadrangle exposes a folded thrust fault that is interpreted to have placed Neoproterozoic rocks over the top of the Paleozoic sequence. As the WLN is traced northward into the adjacent Welcome quadrangle, this folded thrust sheet hosts Neoarchean to Paleoproterozoic orthogneiss and paragneiss in its core—the oldest and possibly also the most deeply exhumed rocks in the state of Nevada (McGrew and Snoke, 2015). These rocks are best exposed in the cirque wall above Angel Lake in the Welcome quadrangle and hence are

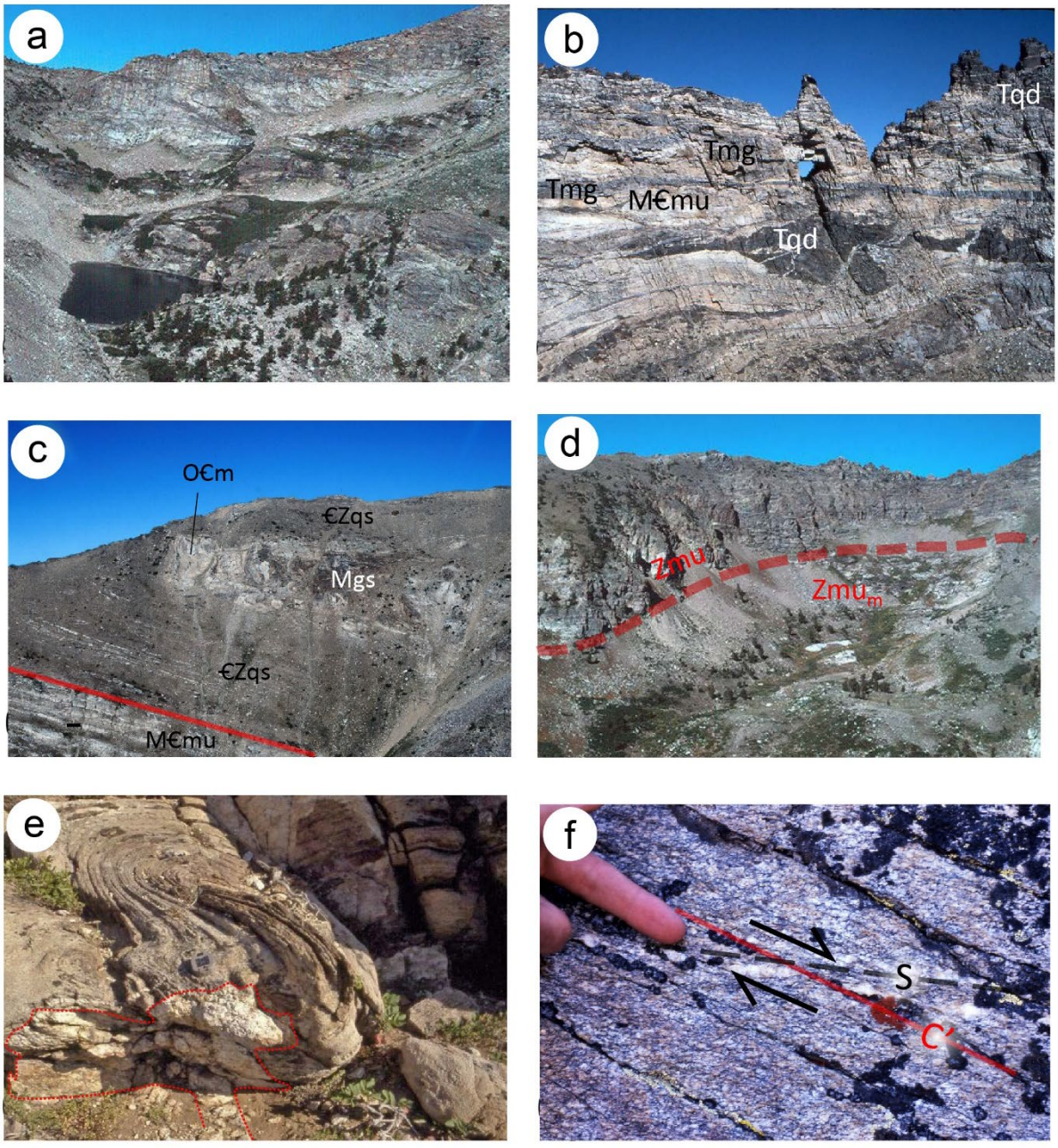

Figure 2. Photographs of field relationships in the Humboldt Peak quadrangle (unit symbols as in the map plate throughout). (a) Steele Lake, a characteristic cirque lake on the steep eastern flank of the range (photograph by A.W. Snoke). (b) The Hole-in-the-Mountain, a notable local land mark formed by the erosion of a marble enclave (M€mu) in more resistant orthogneiss (Tqd & Tmg) in the western arête of Lizzies Basin (photograph by A.W. Snoke). (c) Hinge zone of the Winchell Lake fold-nappe in the cirque wall west of Winchell Lake (photograph by A.W. Snoke). (d) South cirque of Lizzies Basin annotated with red dotted line to delineate the upper boundary of the migmatite complex of Lizzies Basin; note transition in outcrop style from rounded white outcrops of severely migmatized rock (Zmu_m) beneath the 67% leucogranite isopleth to the more strongly layered outcrop style of the gneisses above the migmatitic front (Zmu) (photograph by A.W. Snoke). (e) Re-folded fold in marble; note leucogranitic intrusion in lower left apparently cutting older fold but probably partly involved in final phase of folding (photograph by A.J. McGrew). (f) Protomylonitic orthogneiss showing well-developed normal-sense shear bands (C′-planes) transecting grain shape foliation (S-planes); inferred shear-sense indicated by half-arrows (photograph by A.J. McGrew).

referred to as the gneiss complex of Angel Lake (Lush et al., 1988). This complex consists of the Neoarchean to Paleoproterozoic gneiss, including the paragneiss of Angel Lake and the orthogneiss of Chimney Rock (Premo et al., 2008; McGrew and Snoke, 2010, 2015; Premo et al., 2010; McGrew and Premo, 2011; Premo et al., 2014). Folded around the Neoarchean to Paleoproterozoic gneiss is a sequence of mostly Neoproterozoic paragneiss (the paragneiss of Greys Peak) that is exposed near the northwestern corner of the Humboldt Peak quadrangle where it wraps around the closure of the WLN.

Folded around the Precambrian gneiss complex of Angel Lake is a sequence of quartzite, pelitic schist, and marble interpreted to represent a profoundly attenuated, multiply metamorphosed and polyphase-deformed section of the Neoproterozoic to Paleozoic sequence of the eastern Great Basin. Curiously, the inferred stratigraphic facing direction of this sequence is upward toward the Precambrian basement rocks in the core of the WLN. In other words, the Precambrian gneiss complex of Angel Lake appears to face outward as would be expected for an anticlinal fold, but the metamorphosed miogeoclinal sequence faces inward as would be expected for a syncline. This perplexing relationship is interpreted by McGrew and Snoke (2015) to represent the folding of a major pre-metamorphic thrust fault that emplaced an overturned section of Precambrian rocks over the metamorphosed Neoproterozoic to Paleozoic section as illustrated in fig. 3. This deeply penetrating thrust system may correlate with the inferred Windermere Thrust system of Camilleri and Chamberlain (1997). Unfortunately, due to the intensity and complexity of subsequent deformational overprinting, no evidence is preserved to record the original vergence direction of this inferred pre-metamorphic thrust. However, if the fault does indeed correlate with the Windermere thrust, the transport direction before being re-folded by the WLN would likely have been toward the east or southeast. Though extraordinary subsequent plastic attenuation has now thinned this composite structural section to less than 700 m, this pre-metamorphic, pre-WLN thrust fault was probably originally responsible for the deep tectonic burial of the Neoproterozoic to upper Paleozoic sequence. This pre-WLN thrust system was probably emplaced synchronously with an older generation of isoclinal folds (*F(n-1)*) that were later refolded by the WLN and associated Fn generation outcrop-scale folds (figs. 2c and 2e) (McGrew, 1992). This older, *F(n-1)* generation of folding may have been responsible for the over-turning of the Neoarchean to Neoproterozoic gneiss complex of Angel Lake as illustrated in figure 3. Subsequent Cenozoic extensional shearing probably transposed the hingeline of the WLN into its present WNW trend, and detachment faulting is inferred to have excised the overlying superstructure (fig. 3).

At higher structural levels in both the Lizzies Basin complex and the WLN, the EHR is increasingly overprinted by WNW-directed mylonitic fabrics (fig. 2f). Although there is no sharply defined base to the mylonitic shear zone, the mylonitic character of the gneisses diminishes greatly with depth and there is a reversal in bulk shear-sense from WNW-directed normal-sense shear at higher structural levels to mostly ESE-directed normal-sense shear at deeper structural levels (McGrew, 1992; McGrew and Casey, 1998) (see map plate, cross section B–B'). Extensional mylonitic fabrics overprint and therefore postdate Eocene and Oligocene intrusive rocks (fig. 2f). However, mylonitization must have been mostly complete by the time the rocks cooled through $^{40}Ar/^{39}Ar$ biotite closure temperatures (300 ± 50°C) in the early Miocene (McGrew and Snee, 1994); thus, mylonitic deformation is bracketed between mid-Oligocene and early Miocene.

Along much of the east flank of the EHR an apron of Quaternary glacial and alluvial-fan deposits mantle and partially obscure the range-front fault. Nonetheless, in the southern part of the quadrangle the farthest east extent of basement rock is delineated by an inferred Quaternary fault scarp (also recognized by Dohrenwend et al., 1991a). Also, in the Welcome quadrangle to the north, the range-front fault is interpreted to cut an Angel Lake stage moraine, indicating that the most recent fault rupture was probably <15,000 years ago (McGrew and Snoke, 2015).

Finally, paralleling the EHR to the east is a smaller, east-tilted horst block forming a line of hills represented by Signal Hill in the northeastern Humboldt Peak quadrangle and a smaller hill just to its south. This line of hills extends northward to Clover Hill in the adjacent Welcome and Wells quadrangles, where the fault bounding the east side of the horst block is marked by inferred Quaternary scarps, and has been called the Clover Hill fault (Dohrenwend et al., 1991b; Henry and Colgan, 2011; McGrew and Snoke, 2015). Henry and Colgan (2011) hypothesized that the 2008 Wells earthquake occurred on a "blind" segment of this fault projected to the north. Tracing the Clover Hill fault southward, it is not clear whether it terminates in the east-central part of the Humboldt Peak quadrangle or whether it extends farther south to merge with the EHR range-front fault system in the southern part of the quadrangle.

STRUCTURAL ANALYSIS

As detailed in the section on structural architecture above, from shallower to deeper structure of the large-scale structure of the Humboldt Peak quadrangle is controlled by the following major features:

a. The range-bounding normal fault systems on both sides of the EHR, and along the east side of the Signal Hill horst block (all inferred to have been active during Pleistocene to early Holocene time).
b. Clover Valley basin on the east side of the EHR, which is underlain in the north-central part of the quadrangle by Miocene sedimentary and volcanic rocks, all cut by brittle normal faults.
c. A thick zone of WNW-directed protomylonitic to mylonitic rocks several hundred meters thick increasingly well developed at high structural levels in the EHR.

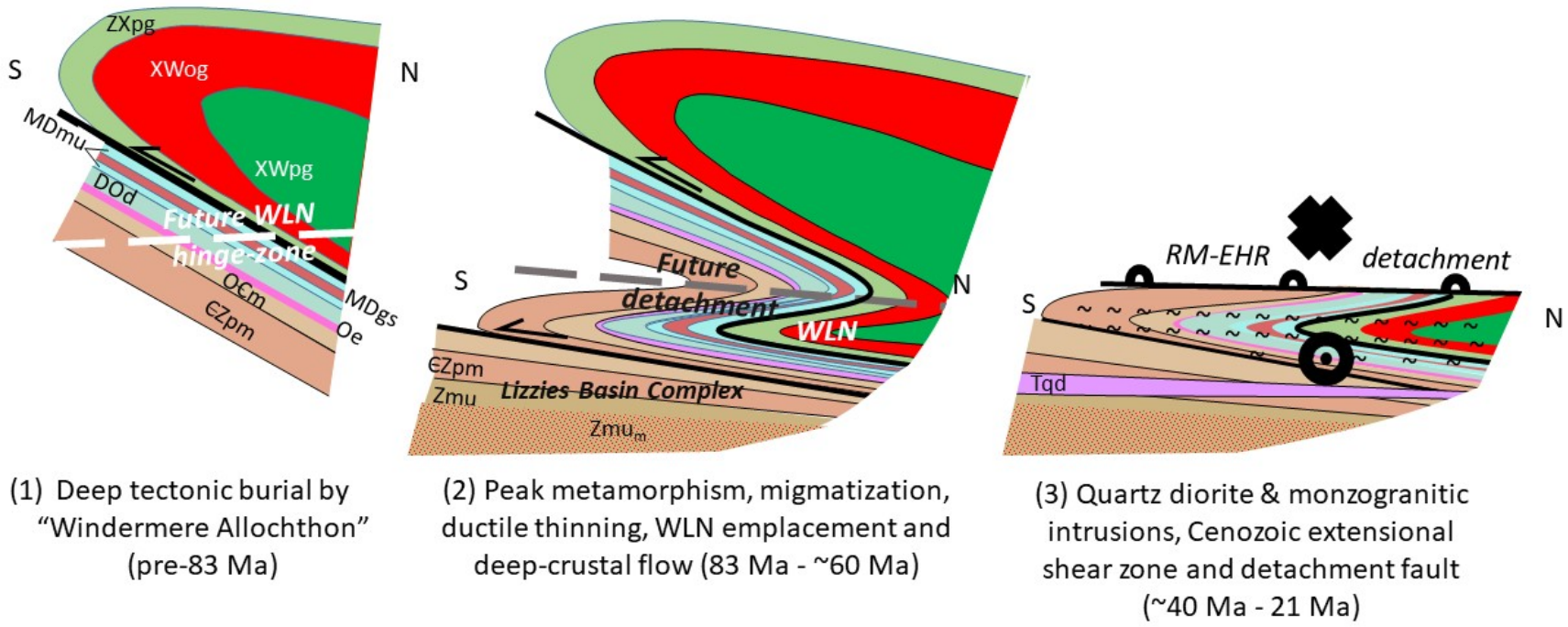

Figure 3. Cartoon illustrating inferred structural evolution of northern EHR in three stages: (1) Pre-83 Ma: F(n-1) folding and emplacement of Precambrian Angel Lake gneiss complex resulting in deep tectonic burial and kyanite zone metamorphism of Neoproterozoic to Paleozoic sequence (Note: the Windermere allochthon is inferred to have been transported to the SE based on regional relationships); (2) 83 Ma to ~60 Ma: Widespread migmatization, peak metamorphism (sillimanite grade), extreme plastic attenuation during deep-crustal flow, and emplacement of WLN contemporaneous with Fn folding; (3) ~40 Ma to Middle Miocene: Cenozoic WNW-directed extensional mylonitic shearing with associated F(n+1) folding, brittle-on-ductile overprinting by RM-EHR detachment fault, and extensional excisement of overlying superstructure. Ductile extensional phase pre-dates 21 Ma whereas brittle extension largely post-dates 17 Ma. (Note transposition of WLN hingeline into parallelism with WNW-directed mylonitic stretching lineation). Units symbols: XWpg - paragneiss of Angel Lake; XWog - orthogneiss of Chimney Rock; ZXpg - paragneiss of Greys Peak; Zmu and Zmu$_m$ - McCoy Creek Group of Lizzies Basin, undivided (migmatitic phase denoted by subscript "m"); €Zpm - Cambrian to Neoproterozoic Prospect Mountain quartzite and McCoy Creek Group, undivided; O€m - Ordovician to Cambrian marble; Oe - Ordovician Eureka Quartzite; DOd - Devonian to Ordovician dolomitic marble; MDmu - Mississippian to Devonian marble, undiivided; MDgs - Mississippian to Devonian graphitic schist (possibly Pilot formation).

d. A metamorphic core of upper amphibolite-facies migmatitic gneiss well exposed throughout the western half of the quadrangle, commonly with protomylonitic zones showing antithetic shear-sense relative to that of the overlying mylonitic zone.
e. In the northwestern part of the quadrangle, a multi-kilometer scale, southward-closing recumbent isoclinal fold (the WLN), cored farther north by the Precambrian gneiss complex of Angel Lake.
f. At least one major pre-metamorphic, pre-WLN thrust fault separating the gneiss complex of Angel Lake from the inferred Neoproterozoic to Paleozoic metasedimentary sequence folded around it.

The sections below elaborate on the detailed structural relationships within and between the major elements of the structural architecture outlined above.

Fold Relationships

The deformational history in the core of the EHR can be subdivided into at least three major fold phases, with the first phase probably coeval with the deep tectonic burial of the Paleozoic metasedimentary section by the Windermere thrust, the second phase synkinematic with emplacement of the WLN, and the third phase being synkinematic with the Cenozoic mylonitic shear zone. All three fold phases are essentially coaxial with each other and with grain-shape lineation in the late Oligocene mylonitic shear zone. Consequently, identifying which of the fold phases is represented in a given outcrop is commonly problematic. Moreover, due to the complexity of the deformation history and the intensity of metamorphism, it is possible that future work may reveal the existence of still older fold phases. Accordingly, in the nomenclature adopted below the WLN-related fold phase is denoted as *Fn*, younger folds as *F(n+1)* and the older fold phase as *F(n-1)*. Despite these complexities, there are rare locations where overprinting fold phases can be recognized (e.g., figs. 2c and 2e). In the case depicted in figure 2e, a leucogranitic intrusion in the lower part of the outcrop cuts the older generation folds (here inferred to be *F(n-1)*) but appears to be at least partly involved in the later fold phase (probably *Fn*).

The older, *F(n-1)* fold phase is poorly understood, but may be synkinematic with the initial phase of tectonic burial represented by the pre-WLN thrust fault that is inferred to have emplaced the Angel Lake gneiss complex over the Neoproterozoic to Paleozoic metasedimentary sequence (fig. 3). The *F(n+1)* fold phase locally affects the late Eocene quartz dioritic rocks and the Oligocene biotite monzogranitic orthogneiss sheets; therefore, it is interpreted to be synkinematic with late Cenozoic ductile attenuation and mylonitic shearing (fig. 4). All three fold phases are essentially coaxial with each other and with mylonitic stretching lineation. Consequently, except in the rare localities where the fold phases are observed overprinting each other or folding orthogneiss bodies of known age, it is commonly difficult or impossible to assign a given fold observed in the field to a particular fold phase.

Foliation throughout the Humboldt Peak quadrangle is predominantly shallowly dipping (averaging 308°, 5°) and is associated with nearly ubiquitous grain shape lineation with an average orientation of 119.5°, 0.4° (fig. 5a). Poles to foliation yield a diffuse girdle with a cylindrical best-fit solution indicating an average fold axis oriented 308°, 0° subparallel to the mean grain shape lineation cited above (fig. 5a). Small-scale fold hinge lines throughout the area show a similar unimodal distribution averaging 297°, 2° (figs. 5a and 5b). Small-scale fold hinge planes also show a unimodal distribution concentrated at 287°, 14°, resembling but slightly steeper than mean grain shape foliation of 308°, 5° (figs. 5a, 5b). In addition to the statistical fold analyses outlined above, map-scale relationships tightly constrain the hinge line and the axial surface of the WLN, which shows a hinge line oriented 295°, 11° and a hinge surface oriented approximately 258°, 15°. The slightly steeper average dip of fold hinge planes and of the WLN itself relative to mean foliation suggests an overall vergence toward the south.

Although most folding is presumably related to the WLN (inferred to be Late Cretaceous in age), numerous folds also affect mylonitic foliation and in a number of localities inferred late Eocene to Oligocene orthogneiss sheets are also at least partly involved in folding (fig. 4). Moreover, as noted above, small-scale fold hinge lines, the pole to the best-fit great circle of poles to foliation, and the hinge line of the WLN are all oriented subparallel to mylonitic stretching lineation (compare figs. 5a and 5b). Consequently, it seems likely that the older folds were partly or wholly transposed by large magnitude extensional strain during late Cenozoic deformation. Therefore, the original orientation of the WLN and associated folds is uncertain.

In addition to the WNW-trending lineations that are ubiquitous throughout the EHR, localized areas at deeper structural levels exhibit a more northerly trending lineation (black filled circles, fig. 5c). Though scarce, enough of these lineations have been observed in the Humboldt Peak quadrangle to estimate a dominant mode at 169°, 2° (fig. 5c). Although the tectonic significance of these cryptic lineations remains uncertain, extensive areas at deep structural levels in the northern Ruby Mountains show a similarly oriented fabric. There, MacCready et al. (1997) interpreted them as a relic of an earlier phase of deep-crustal flow nearly orthogonal to the upper crustal transport direction. MacCready (1996) showed that despite the existence of this nearly orthogonal stretching lineation, the quartz crystallographic preferred orientations from the northerly-lineated terrain nevertheless record a strain pattern attributable to WNW-directed late Cenozoic extensional stretching. Even more rarely, NE-trending lineations can locally be observed on the same foliation surfaces as the WNW-trending lineations (blue triangles in fig. 5c). Again, the tectonic significance of these cryptic lineations is uncertain, but they could represent an overprinted fabric transitional between the WNW-lineated and the SSE-lineated domains (MacCready et al., 1997).

A.

B.

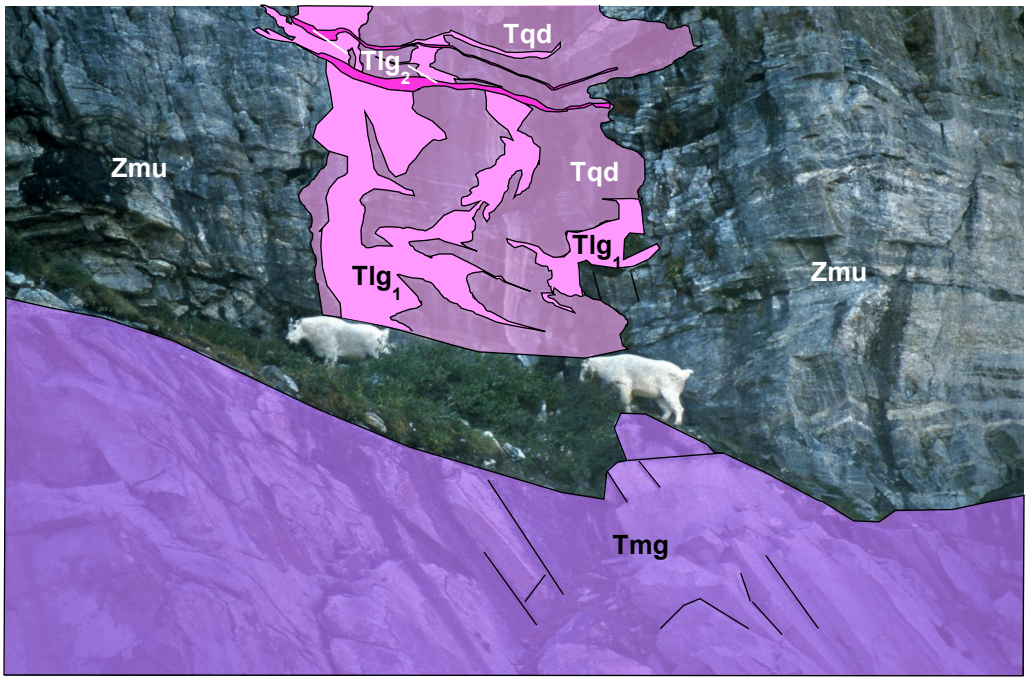

Figure 4. Field photograph (a) with interpretive line drawing and annotations (b) illustrating contact relationships in the Lizzies Basin area between multiple intrusive phases and country rock (Zmu). Mountain goats provide scale. Granitoid orthogneisses range from relatively dark quartz dioritic orthogneiss to cream-colored leucogranitic rock, with older intrusive phases being moderately to strongly foliated whereas later phases are weakly foliated. Foliation in orthogneisses parallels foliation in the country rock, which here consists of McCoy Creek Group quartzitic paragneiss (Zmu); foliation in the paragneiss is accentuated by layered leucosomes inferred to be the oldest magmatic phase (probably Late Cretaceous; not labeled in figure). Cutting most of these foliation-parallel leucosomes is a dark, subvertical, inferred quartz dioritic orthogneiss dike (Tqd, pale purple), which appears to be associated with subvertical leucogranitic dikes (Tlg_1, pink). Both of these older generation granitoids (late Eocene to early Oligocene) are foliated and gently folded with subhorizontal axial planes, suggesting that they were intruded into a subvertical shortening field that probably accommodated a component of plastic thinning during late Eocene to early Miocene extension. Though the quartz dioritic dike appears to cut most foliation-parallel leucosomes, a few of the subhorizontal leucosomes (labeled Tlg_2, magenta) cut the dike. The base of the outcrop consists of biotite monzogranitic orthogneiss (Tmg, pale violet) which appears to cut and therefore post-date the Tqd and Tlg_1 dikes. The younger age of this intrusion is also suggested by its relative lack of cross-cutting leucogranitic bodies, but its shallowly inclined orientation and the local presence of a leucocratic border phase suggests that it likely intruded synchronously with the Tlg_2 sheets.

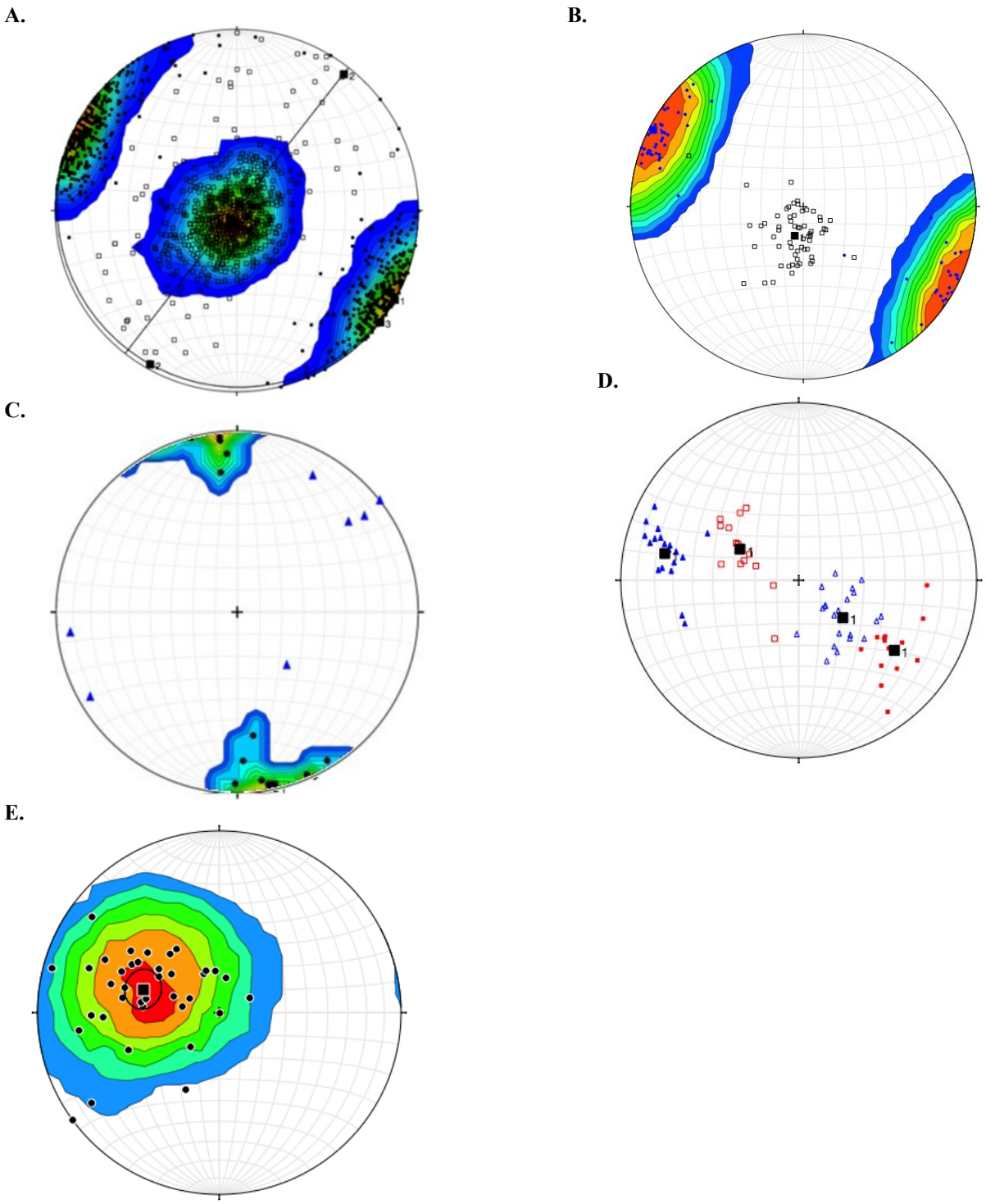

Figure 5. Stereonet plots of structural relationships in the Humboldt Peak quadrangle (all lower hemisphere equal area projections generated with Stereonet 8.0) (Allmendinger et al., 2012) (a) Contoured density plots of grain shape lineations (filled squares) and poles to foliation (open squares) with best-fit great circle. Mean foliation is oriented 308°, 5° with the pole to the best-fit great circle (the mean fold axis) oriented 119.5°, 0.4° subparallel to mean grain shape lineation oriented 308°, 00° (b) Poles to small-scale fold hinge planes (open squares) with a mean orientation of 287°, 14° and contoured density plot of small-scale fold hinge lines (small filled blue circles) oriented on average 297°, 2°. (c) Density contour plot of northerly trending lineations from deep structural levels (filled red circles) with a mean orientation of 169°, 2°. Also shown are rare NE-trending lineations (filled blue triangles). (d) Plot of poles to NW-dipping shear band foliations (C'-planes) in quartzofeldspathic gneiss (blue open triangles) with corresponding hot slickenside lineations (filled blue triangles) versus poles to SE-dipping foliations (red open squares) with their corresponding hot slickenside lineations (red filled squares). NW-dipping shear bands are observed mostly at high structural levels and show a mean orientation of 220°, 26° with hot slickenlineations averaging 281.5°, 24°; conversely, SE-dipping shear bands come mostly from deep structural levels and are oriented on average 028°, 31° with hot slickenside lineations oriented on average 126°, 34°. (e) Density contour plot of poles to bedding from the Signal Hill–Dalton Hill horst block in the NE part of the quadrangle, oriented on average 017°, 36°.

A.

B.

Figure 6. Field photographs of McCoy Creek Group with associated leucogranitic rocks. (a) Folded, striped quartzitic paragneiss intruded by leucocratic granite and pegmatite with randomly oriented coarse laths of biotite. (b) Severely migmatized McCoy Creek Group paragneiss with abundant layer-parallel leucosomes, a cross-cutting leucocratic dike, and a thick leucogranitic sill forming the overlying ledge.

Extensional Deformational History

Overprinting the Mesozoic deformational history is a history of Cenozoic extension that ultimately resulted in the unroofing and exposure of the high-grade metamorphic core. The dominant feature of this history is the RM-EHR mylonitic shear zone and the overlying detachment fault. While the mylonitic shear zone is well developed at higher structural levels, the overlying detachment fault is not exposed in the Humboldt Peak quadrangle, although it is exposed to the west in the Tent Mountain quadrangle (Hurlow, 1987) (fig. 1). The kinematics of deformation during Cenozoic extensional unroofing is expressed by a variety of shear-sense indicators, including S-C-C' relationships, asymmetric mica fish, crystallographic preferred orientations in quartzites, extensional crenulation cleavage in pelitic schists, and shear band fabrics in quartzofeldspathic gneisses. Widespread evidence of crystal-plasticity in feldspars, recrystallization of biotite in shear planes, well-developed evidence of rapid grain boundary migration in quartzites, and high-temperature quartz crystallographic preferred orientations (e.g., McGrew and Casey, 1998) all suggest that a large fraction of the extensional strain occurred under upper greenschist to upper amphibolite-facies conditions. However, locally chlorite occurs along shear planes or in the necks of asymmetrically microboudinaged biotite or hornblende, indicating that extensional deformation continued through lower greenschist facies conditions.

Figure 5d illustrates composite fabric relationships overprinting orthogneissic rocks as defined by C'-planes and extensional shear bands. Since most of the affected orthogneisses are late Eocene to mid-Oligocene in age, the timing of shearing can also be bracketed between the mid-Oligocene and cooling of the terrain through $^{40}Ar/^{39}Ar$ biotite closure temperatures (300 ± 50°C) by earliest Miocene time (see section on Thermochronology and Exhumation below) (McGrew and Snee, 1994). As illustrated in figure 5d, two populations of shear band fabrics are present. At higher structural levels WNW-directed normal-sense shear planes (blue triangles in fig. 5d) form >85% of observed shear-sense indicators; in contrast, at deeper structural levels kinematic indicators show a reversal in bulk shear-sense, with ~70% of shear bands being ESE-directed (red squares). Furthermore, the closer balance between antithetically oriented shear bands at deeper structural levels suggests that the overall strain path increasingly deviates from end member simple shear into the subsimple shear strain regime. In other words, shearing was accompanied by thinning perpendicular to the shear plane and stretching parallel to it. This strain pattern is consistent with a listric normal fault flattening at depth into a shear zone developed on a penetratively stretching deeper crust.

Both the WNW- and the ESE-directed shear bands typically form composite fabric relationships with subhorizontal grain shape foliations ("S-planes") similar in orientation to the bulk foliations illustrated in figure 5a. The mean WNW-directed shear band foliations (or "C'-planes") typically occur in micaceous quartzofeldspathic gneisses and are marked by "hot slickenside" lineations defined by microscopic smears of recrystallized biotite and/or comminuted feldspars. The WNW-dipping shear band foliations yield a mean orientation of 220°, 26° with hot slickenside lineations averaging 281.5°, 24°; in contrast, ESE-directed shear bands average 028°, 31° with hot slickenside lineations averaging 126°, 34° (fig. 5d).

As noted above, the Humboldt Peak quadrangle does not expose the Ruby-East Humboldt detachment fault. However, inferred upper plate sedimentary and volcanic rocks are dropped down against the high grade terrain by the late Miocene to Quaternary, east dipping, high-angle normal fault system that delineates the east flank of the range. These exposures form a line of hills in the NE part of the quadrangle that can be traced northward into the adjacent Welcome quadrangle where correlative rocks on the west flank of Clover Hill are observed to be rotated down against the detachment fault (McGrew and Snoke, 2015). Consequently, the ESE dip of these strata, averaging 017°, 36° (fig. 5e), is interpreted to reflect their rotation down against the detachment fault, which is inferred to underlie them at a shallow depth (map plate, section B–B').

The McCoy Creek Group of Lizzies Basin

Most rock units exposed in the Humboldt Peak quadrangle have been extensively discussed in the text accompanying the adjacent Welcome quadrangle (McGrew and Snoke, 2015); one exception is the McCoy Creek Group of Lizzies Basin (fig. 6). The deeper structural levels in the west-central and southwestern part of the Humboldt Peak quadrangle (especially from Lizzies Basin southward) consist predominantly of a thick, heterogeneous sequence of impure metaquartzite and metapsammitic paragneiss (fig. 4), pelitic schist, marble and calc-silicate rock inferred to correlate with the Neoproterozoic McCoy Creek Group (Misch and Hazzard, 1962; Miller, 1983). This sequence contrasts with the above-described paragneiss of Greys Peak in the absence of fuchsitic quartzite, the rarity of orthoamphibolite bodies, the presence of distinct horizons of marble, and the greater abundance of quartzite in contrast to more micaceous and/or feldspathic varieties of metapsammite. Also in the upper part of the sequence is at least one mappable horizon of brown-weathering bt-sill-gt pelitic schist that may correlate with McCoy Creek unit H (the Osceola Argillite) of Misch and Hazzard (1962) (see table 1 for a list of mineral abbreviations used in this report). Locally, especially at deeper stratigraphic levels in Lizzies Basin, the quartzite units contain thin, more feldspathic interlayers imparting a distinctive striped aspect to some of the rock (fig. 6a). Like other units in the high grade metamorphic core, the original stratigraphic thickness of the McCoy Creek Group of the Lizzies Basin gneiss complex is unknown, but its structural thickness exceeds 1000 m. Therefore, it appears that units in the Lizzies Basin gneiss complex are far less attenuated than those farther north in the WLN.

Table 1. Mineral abbreviations utilized in this report.

Mineral	Abbrev.	Mineral	Abbrev.	Mineral	Abbrev.
Amphibole	amph	Garnet	gt	Quartz	qz
Apatite	ap	Graphite	gr	Rutile	ru
Biotite	bt	Hornblende	hb	Scapolite	scap
Calcite	cc	Ilmenite	ilm	Sillimanite	sill
Cordierite	cd	Kyanite	ky	Spinel	sp
Corundum	crn	Monazite	mnz	Staurolite	st
Chlorite	chl	Muscovite	mu	Titanite	ttn
Diopside	di	Orthoamphibole	oa	Tremolite	tr
Epidote	ep	Plagioclase	pl	Zircon	Zr
		K-feldspar	Ksp		

The marble units within the Lizzies Basin gneiss complex commonly form three or more distinct horizons, and consist most commonly of coarse white marble with >90% calcite, or, less commonly, of calc-silicate-bearing, cream or pale yellow-weathering marble. They contrast with the overlying inferred Paleozoic carbonate in that they lack dolomitic layers and are typically distinctly thinner, commonly <6 m thick, although the highest McCoy Creek Group marble unit beneath Humboldt Peak in the southwestern part of the quadrangle ranges up to 120 m in thickness. Additionally, carbon isotope investigations of these marble units record anomalously high $\delta^{13}C$ values ranging up to 12‰ that contrast strongly with the more normal carbon isotope values (0 to -2 ‰) of the inferred Paleozoic marble sequence (Wickham and Peters, 1993). These anomalously high $\delta^{13}C$ values are inferred to be primary or diagenetic in origin and strongly support correlation with high $\delta^{13}C$ McCoy Creek Group marble units in the Pilot and Schell Creek ranges, and with high $\delta^{13}C$ Ediacaran carbonates worldwide (Wickham and Peters, 1993).

Due to the high metamorphic grade and structural complexity of field relationships in the East Humboldt Range, it is difficult to precisely locate and map the boundary between the McCoy Creek Group and the overlying Prospect Mountain Quartzite (Hague, 1883); consequently, the contact between these two units was arbitrarily defined at the top of the uppermost marble horizon in the McCoy Creek Group. This definition of the boundary includes the upper part of the McCoy Creek Group with the Prospect Mountain Quartzite, leading to the dual designation on the map of Prospect Mountain Quartzite and McCoy Creek Group, undivided. Relatively pure quartzite is more abundant in the Prospect Mountain Quartzite and the extent of migmatization is correspondingly less. However, like the underlying McCoy Creek Group, Prospect Mountain Quartzite is locally migmatitic, with more pelitic and/or feldspathic horizons harboring a higher percentage of leucosome than the purer quartzite layers.

Migmatitic Phase

Like other units in the EHR, the McCoy Creek Group is migmatitic, and the proportion of leucogranitic rock increases gradationally but abruptly and dramatically at elevations below approximately 9000 ft (~2750 m) (see boundary mapped as red hachured line in plate 1) (fig. 2d; fig. 6). In general, at structural levels above this boundary the proportion of leucogranitic rock, as visually estimated based on area of exposure, is less than 33% whereas beneath this boundary the rocks typically contain greater than 67% leucogranite (and locally up to 90% or more). In the area just above this important boundary (the 67% leucogranite isopleth) 10 m-scale, subvertical finger-like protrusions of leucogranite are commonly observed and appear to represent small diapiric masses of leucogranite sourced from the underlying severely migmatized zone. Sill-like bodies of leucogranite are widespread both above and below the 67% leucogranite isopleth, but tend to be more discrete and therefore more easily mapped above this contact due to their stronger contrast with the surrounding metasedimentary rock. Migmatites are commonly subhorizontally layered (fig. 6b), and are particularly concentrated in less "clean" parts of the stratigraphy; in such areas lenses, pods or continuous layers of leucosome ranging from cm-scale to meter-scale are commonly bounded or interdigitated with dark selvages ("melanosomes") of concentrated biotite and sillimanite. Accordingly, much of the leucogranite is inferred to be in source, although not necessarily strictly in situ. Locally, marble horizons a few meters thick can be traced across the 67% leucogranite isopleth into the strongly migmatized zone, where they become dramatically thinner and locally evince wholesale conversion to diopside-grossular garnet gneiss. Layers and pods of such diopside-rich rock are commonly mantled by reaction coronas millimeters to centimeters thick enriched in actinolitic amphibole.

CONDITIONS OF METAMORPHISM

Metamorphic conditions in the northern EHR have been extensively investigated and discussed in previous publications and are only briefly summarized here (table 2) (Hurlow et al., 1991; Peters and Wickham, 1994; McGrew et al., 2000; McGrew and Snoke, 2015; Hallett and Spear, 2014, 2015). The northern EHR consists of a migmatitic upper amphibolite-facies metamorphic core with localized greenschist facies overprints that are synkinematic with late-

Table 2. Thermobarometric results from the Humboldt Peak quadrangle summarized from McGrew et al. (2000). Map locations in parentheses following sample numbers refer to sample locations labeled with circled numbers on the map plate. All latitudes and longitudes are in the WGS 1984 datum.

Sample (Location)	Latitude	Longitude	Elevation	Assemblage	P (kb)	T (ºC)
AJM.WL3 (1)	40.98915°	-115.10443°	3133 m (10,280 ft)	bt+sill+gt+qz+plag+ru+ilm	7.0 ± 1.0	653 ± 96
AJM.WL1 (2)	40.98561°	-115.09717°	2731 m (8960 ft)	bt+sill+gt+qz+Ksp+pl+ru	8.4 ± 0.9	740 ± 50
AJM.WL2 (3)	40.98368°	-115.09648°	2670 m (8760 ft)	bt+gt+st+cd+sp+pl+oa+ ru+ilm+crn±qz+sil+chl	6.1 ± 0.8	642 ± 23
MP.WL8					6.3 ± 1.0	645 ± 88
AJM.LB1 (4)	40.94739°	-115.10281°	2640 m (8660 ft)	bt+sil+gt+qz+ksp+pl+ru	8.6 ±0.9	751 ± 54
AJM.LB2 (5)	40.94429°	-115.11405°	2731 m (8960 ft)	bt+sill+gt+qz+plag+ilm+(chl)	8.0 ± 1.2	717 ± 115
MP.LB132 (6)	40.93205°	-115.12496°	3200 m (10,500 ft)	gt+bt+mu+sil+qz+ilm+ru	5.9 ± 0.9	635 ± 106

stage extensional mylonitization and post-mylonitic extensional jointing. Metapelitic rocks on the upper limb of the WLN locally preserve pre-peak metamorphic kyanite (always mantled by sillimanite). In contrast, on the lower limb of the fold the fossil kyanite-bearing assemblages are completely replaced by peak metamorphic assemblages consisting of bt + sill + gt ± Ksp (McGrew et al., 2000); thus the kyanite-out isograd approximately parallels the hinge zone of the WLN. In addition, leucogranitic rock inferred to have been generated and injected synchronously with peak sillimanite-zone metamorphism increases in abundance with depth, and thus isopleths of leucogranite abundance also transect the WLN subparallel to its hinge zone. Based on the observation that layer-parallel bodies of leucogranite are folded around the WLN whereas isopleths of leucogranite abundance cut the WLN, McGrew et al. (2000) inferred that the Winchell Lake fold formed synkinematically with peak metamorphism, partial melting, and leucogranite injection. Consequently, they inferred that a Late Cretaceous U-Pb zircon ID-TIMS age of 84.8 ± 2.8 Ma on a pegmatitic leucogranite folded around the nose of the WLN was broadly synkinematic with both fold-nappe emplacement and migmatization as well as the associated sillimanite zone peak metamorphism (sample RM18 located at site B labeled with a triangular box on the map plate) (McGrew et al., 2000). Subsequent re-dating of the same sample by SHRIMP U-Pb zircon yields a statistically similar age of 83.5 ± 1.3 Ma (Premo et al., 2014) thus disconfirming a suggestion by Hallett and Spear (2014, 2015) that the original ID-TIMS age may have incorporated an inherited component. However, it remains possible that this particular body of leucogranite formed during an earlier phase of Late Cretaceous migmatization before the final emplacement of the WLN was completed in the post-77-Ma time frame preferred by Hallett and Spear (2015) (see below).

Building on the work of McGrew et al. (2000), Hallett and Spear (2014, 2015) documented independent P-T-t paths for the Lizzies Basin complex and the upper limb of the WLN. They present integrated thermobarometric and U-Pb monazite and zircon SHRIMP data indicating that prograde metamorphism in the Lizzies Basin complex began between ~86.8 Ma and 97.5 Ma and reached a peak at ~8 kb, 775°C before beginning crystallization of zircon and later of monazite on the decompressional path between 88.8 Ma and 77.1 Ma (Hallett and Spear, 2015). In contrast, peak metamorphism at ~10 kb, 700°C, on the upper limb of the WLN is bracketed between the growth of monazite cores under pre-peak conditions of 380°–450°C at 82.8 ± 2.8 Ma and crystallization of zircon and monazite beginning after 77.1 Ma at conditions of ~7 kb, 750°C (Hallett and Spear, 2014, 2015). The P-T-t paths for both the Lizzies Basin complex and the WLN converge after ~60 Ma, suggesting that the WLN had been emplaced in its current configuration by the early Paleocene. In addition, both the Lizzies Basin complex and the WLN preserve evidence for an over-printing thermal event at conditions of 4–5 kb, 510°–570°C documented by renewed growth of monazite and zircon contemporaneous with late Oligocene quartz dioritic to granitic magmatism between ~40 Ma and ~30 Ma (Hallett and Spear, 2015; Drew, 2013; Wright and Snoke, 1993). Thermobarometric investigation from high levels in the mylonitic zone in the adjacent Tent Mountain quadrangle constrains the lower pressure part of the P-T-t path, recording metamorphism syntectonic with extensional mylonitization at 550–600°C and 3–4 kb (Hurlow et al., 1991). In addition, Al-in-hornblende barometry indicates that hornblende in the 40-Ma hornblende-biotite quartz diorite sill crystallized at pressures of 4.5–5.5 kb, consistent with the above P-T-t path (McGrew and Snee, 1994).

Integrating currently available results, the following generalizations are apparent:

1) Relict kyanite zone metamorphism is preserved only on the upper limb of the WLN and records an episode of rapid tectonic burial bracketed between ~85 Ma and ~77 Ma.
2) Sillimanite zone peak metamorphism at temperatures ≥750°C and pressures of 7–10 kb in both the Lizzies Basin complex and the WLN occurred synchronously with Late Cretaceous to Paleocene migmatization beginning at least by ~75 Ma and possibly as early as 83 Ma.

Table 3. $^{40}Ar/^{39}Ar$ results from the Humboldt Peak quadrangle after McGrew and Snee (1994). The map locations labeled in bold face correspond with the points in square text boxes on Plate 1. "Near-plateau" ages calculated on <50% of the radiogenic ^{39}Ar are enclosed by quotation marks. Latitudes and longitudes in decimal degrees, WGS 1984 datum.

Map Location (Sample #)	Rock Type (comments)	Longitude Latitude	Elevation	Mineral	Integrated Age (Ma)	Plateau Age (Ma)	Isochron Age (Ma)	$^{40/36}Ar_i$
1 (880706-2A)	Amphibolite (minor excess Ar on step-spectrum from ~48 Ma to ~29 Ma)	-115.09647° 40.99975°	9980 ft (3042 m)	Hb Bt	44.6 ± 0.2 21.9 ± 0.2	n.a. 22.1 ± 0.2	38.0 ± 0.5 22.53 ± 0.06	207 ± 10 267 ± 2
2 (880709-2)	Mu schist	-115.10428° 40.99931°	10,300 ft (3140 m)	Mu	21.9 ± 0.2	21.7 ± 0.2	21.8 ± 0.1	295 ± 3
3 (RM19)	Hb-bt quartz diorite (excess Ar)	-115.09105° 40.99494°	8640 ft (2633 m)	Hb Bt	43.6 ± 0.4 23.43 ± 0.10	n.a. "23.17 ± 0.07"	36 ± 1 23.6 ± 0.2	339 ± 10 284 ± 5
4 (890709-2A)	Hb bt quartz diorite orthogneiss (excess Ar; minimum age step at 45.6 Ma)	-115.09750° 40.97547°	9060 ft (2760 m)	Hb	92.0 ± 0.7	"< 45.6 Ma"	n.a.	n.a.
5 (880805-3)	Bt-sill-gt schist (step release from ~30-35 Ma to ~ 20-25 Ma)	-115.10281° 40.94739°	8660 ft (2640 m)	Bt	26.74 ± 0.08	n.a.	27.1 ± 0.1	260 ± 4
6 (890718-3)	Amphibolite (minor excess argon)	-115.10697° 40.94286°	9000 ft (2743 m)	Hb	45.2 ± 0.3	n.a.	35.8 ± 0.7	342 ± 19
7 (890725-2)	Amphibolite	-115.11531° 40.94167°	9900 ft (3018 m)	Hb	57.9 ± 0.8	49 ± 1	50.3 ± 0.8	222 ± 24

3) Emplacement of the WLN began at the same time as or after Late Cretaceous peak metamorphism, and probably accompanied the early phases of decompressional metamorphism; it appears to largely or wholly postdate the tectonic burial phase.
4) Decompression from pressures as high as 10 kb to pressures of approximately 4–6 kb predated the onset of large-scale Neogene extension.
5) A late Eocene to Oligocene thermal pulse at conditions of 4–5 kb, 510°–570°C preceded the final phase of unroofing in the late Cenozoic.

Constraints bearing on the final phase of unroofing are discussed below.

THERMOCHRONOLOGY AND EXHUMATION

In addition to the quantitative thermobarometry described above, the timing and progressive exhumation of the EHR is constrained by $^{40}Ar/^{39}Ar$ hornblende and biotite thermochronology (McGrew and Snee, 1994). $^{40}Ar/^{39}Ar$ geochronological results from the Humboldt Peak quadrangle are summarized in table 3. As documented by McGrew and Snee (1994) structural levels above ca. 2850 m (9350 ft) mostly yield $^{40}Ar/^{39}Ar$ hornblende cooling ages of ≥50 Ma, whereas deeper structural levels did not cool through the $^{40}Ar/^{39}Ar$ hornblende closure temperature range of ~480–580°C until 30–38 Ma. One amphibolite sample from shallower structural levels (880706-2A, locality 1 in table 3) showed evidence of partial resetting in the 30–38 Ma time frame, but this sample was collected adjacent to a relatively large body of Oligocene biotite monzogranitic orthogneiss. These results are generally consistent with the thermobarometric results summarized above (McGrew et al., 2000; Hallett and Spear, 2014, 2015).

Regionally, cooling through $^{40}Ar/^{39}Ar$ biotite closure temperatures of 300 ± 50°C occurred diachronously from ESE to WNW across the RM-EHR, from >35 Ma in the southeast to ~20 Ma in the northwest (Kistler et al., 1981; Dallmeyer et al., 1986; McGrew and Snee, 1994). In the Humboldt Peak quadrangle, this pattern is reflected by slightly older cooling ages in the southern part of the quadrangle younging toward the north. Whereas deep structural levels in Lizzies Basin cooled through $^{40}Ar/^{39}Ar$ biotite closure at 27.1 ± 0.1 Ma, mica cooling ages farther north range from a biotite cooling age of 23.6 ± 0.2 Ma to a muscovite cooling age of 21.8 ± 0.1 Ma. The WNW-directed cooling age pattern across the RM-EHR is consistent with WNW-directed extensional shear-sense indicators in the mylonitic zone and the overprinting of the mylonitic fabrics on Oligocene monzogranitic orthogneisses. However, despite the above cooling history, a variety of evidence from adjacent areas indicates that final exhumation of the EHR and exposure at the surface did not occur until after mid-Miocene time (e.g., Haines and van der Pluijm, 2010; McGrew and Snoke, 2015).

SUMMARY AND CONCLUSIONS

The Humboldt Peak quadrangle exposes the structurally deepest levels of the Ruby Mountains-East Humboldt Range metamorphic core complex, and as such preserves crucial relationships for understanding crustal structure and processes of deep-crustal deformation during the Late Cretaceous to Miocene tectonic evolution of the northeastern Great Basin. In particular, it exposes a multi-kilometer scale, southward-closing recumbent fold-nappe (the WLN) that formed in Late Cretaceous time during upper amphibolite facies peak metamorphism and migmatization. This fold-nappe transported what may be Nevada's most deeply exhumed rocks—with peak pressures ranging up to 10 kb and peak temperatures exceeding 750°C. Fold-nappe emplacement and metamorphism were also accompanied by widespread partial melting and lit-par-lit migmatization (McGrew et al., 2000; Hallett and Spear, 2014, 2015). In addition, the Humboldt Peak quadrangle exposes >500 m of late Cenozoic protomylonitic to mylonitic rocks that overprint the Late Cretaceous structures and define the RM-EHR extensional mylonitic shear zone. Flanking the EHR to the east is a large-scale, Quaternary normal fault that separates the high grade rocks from unmetamorphosed hanging wall strata ranging from Paleozoic sedimentary rocks to Neogene volcanics. These ESE-tilted strata are interpreted as a down-dropped vestige of the hanging wall rocks that once overlay the East Humboldt Range above the RM-EHR detachment fault.

GEOLOGIC UNITS

Qm Manmade deposits (Anthropocene) Disturbed ground and compacted fill overlain by asphalt along Clover Valley Road. Thickness <3 m (10 ft).

Qu Quaternary units, undivided (Holocene to Pleistocene) Unconsolidated alluvium, colluvium, talus, landslide deposits, and glacial deposits, in cross section only.

Qya Younger alluvium (upper Holocene) Unconsolidated silt, sand, and gravel of fluvial origin filling active stream channels and adjacent flood plains, mostly inset into coalesced alluvial fans on the eastern flank of the East Humboldt Range. Clasts include a wide variety of rock types recognizable from the mountains to the west. Thickness <8 m (26 ft).

Qls Landslide deposit (Holocene) Coarse, unconsolidated debris consisting of local bedrock and/or remobilized glacial deposits; forms hummocky topography. Thickness uncertain and probably highly variable.

Qt Talus deposit (Holocene) Coarse (10 cm to >3 m), angular rock debris with little fine matrix and sparse vegetation, mostly occupying steep slopes beneath cliffs or moderate slopes in alpine environments subject to strong frost action. Thickness highly variable, mostly <10 m (33 ft).

Qc Colluvium (Holocene) Soil consisting of poorly sorted silt, sand, gravel, and locally some talus mantling steep slopes with enough fine matrix to support grassy or brushy vegetation. Thickness <3 m (10 ft).

Qoa Older alluvium (Pleistocene) Weakly consolidated or unconsolidated silt, sand, and gravel forming alluvial-fan surfaces away from or above active stream channels. This unit veneers terraces underlain by bedrock on the eastern flank of the northern East Humboldt Range. Clasts include a wide sampling of rock types recognizable from the adjacent mountains. Maximum thickness is unknown, but in most areas is estimated at <10 m (33 ft).

Qg Glacial deposits (Pleistocene) Chiefly includes morainal deposits, Lamoille and Angel Lake stages (Sharp, 1938; Wayne, 1984) undivided. Thickness is unconstrained and highly variable, estimated up to 80 m (100 ft).

Inferred Disconformity

Th Humboldt Formation (Miocene) The Humboldt Formation is exposed in the north-central part of the quadrangle in just one locality along Wiseman Creek. At this locality it includes (from its base): an approximately 2 m thick layer of pyroclastic fall overlain by approximately 1.3 m of laminated, fine-grained volcanic ash and ashy sediment forming graded beds ranging from a few millimeters to approximately 7 cm thick. Overlying the laminated interval is a second massive pyroclastic fall >1 m thick. The laminated interval is locally affected by soft-sediment folding, and the lower part of the sequence is cut by a small-scale normal fault oriented 049°, 66° with a down-to-NE dip separation of approximately 25 cm. C.D. Henry (pers. comm.) reports a maximum $^{40}Ar/^{39}Ar$ sanidine age for this unit of 15.97 ± 0.09 Ma based on the mean of the three youngest grains; however, the presence of older grains ranging in age to 25 Ma implies that the unit is of mixed provenance, and it is possible that the actual depositional age could be slightly younger (table 4; fig. 7). The underlying strata are not exposed at this locality, but strata approximately 1 km to the west dip ~40° SE as do strata approximately 2 km to the north in the southern Welcome quadrangle. Consequently, faults are inferred to separate the flat-lying Humboldt Formation exposures at Wiseman Creek from the more steeply dipping Miocene strata to the north and west, but the geometry of the inferred fault systems is problematic (see map plate). Still farther north, in railroad cuts west of Wells, Nevada, the Humboldt Formation contains steeply dipping tuffs with ages as young as 8.3 ± 0.9 Ma (Mueller, 1992). Consequently, the Humboldt Formation exposed in the Welcome quadrangle appears to be much thicker and longer lived than the Humboldt Formation exposed in the Humboldt Peak quadrangle. The basal contact of the Humboldt Formation at Wiseman Creek is not exposed and the overlying material is interpreted as older alluvium. Therefore, the total thickness of the unit in this area is unconstrained.

Table 4. $^{40}Ar/^{39}Ar$ analytical data for Sample 040731-1A. Analysis by C.D. Henry at the New Mexico Geochronology Research Laboratory New Mexico Institute of Mining and Technology (http://geoinfo.nmt.edu/labs/argon/home.html)

ID	$^{40}Ar/^{39}Ar$	$^{37}Ar/^{39}Ar$	$^{36}Ar/^{39}Ar$ (x 10^{-3})	$^{39}Ar_K$ (x 10^{-15} mol)	K/Ca	$^{40}Ar^*$ (%)	Age (Ma)	±1□ (Ma)		
040731-1A, san, J=0.0039176±0.02%, D=1±0, NM-283E, Lab#=64957										
06	2.295	0.0070	0.1826	0.825	72.6	97.7	15.954	0.076		
03	2.314	0.0032	0.2377	0.539	159.5	97.0	15.97	0.11		
04	2.280	0.0035	0.1126	0.888	144.8	98.5	15.990	0.070		
05	*2.323*	*0.0077*	*0.0798*	*2.313*	*66.4*	*99.0*	*16.369*	*0.027*		
18	*3.310*	*0.0083*	*0.2287*	*2.457*	*61.7*	*98.0*	*23.054*	*0.029*		
11	*3.527*	*0.0095*	*0.1159*	*5.547*	*53.6*	*99.0*	*24.828*	*0.013*		
02	*3.514*	*0.0248*	*0.0716*	*0.956*	*20.6*	*99.5*	*24.841*	*0.066*		
08	*3.960*	*0.0184*	*1.466*	*0.205*	*27.8*	*89.1*	*25.08*	*0.31*		
16	*3.833*	*0.0330*	*1.007*	*0.303*	*15.5*	*92.3*	*25.14*	*0.22*		
07	*3.621*	*0.0108*	*0.2645*	*1.512*	*47.4*	*97.9*	*25.186*	*0.043*		
12	*3.669*	*0.0463*	*0.3182*	*1.041*	*11.0*	*97.5*	*25.430*	*0.063*		
10	*3.719*	*0.0183*	*0.1756*	*3.906*	*27.9*	*98.6*	*26.069*	*0.018*		
09	*4.008*	*0.0238*	*0.5131*	*1.921*	*21.4*	*96.3*	*27.412*	*0.038*		
19	*4.103*	*0.0135*	*0.1655*	*6.751*	*37.8*	*98.8*	*28.799*	*0.013*		
01	*4.454*	*0.0053*	*0.0230*	*12.590*	*95.8*	*99.9*	*31.568*	*0.006*		
14	*4.837*	*0.0043*	*0.4054*	*1.284*	*118.5*	*97.5*	*33.472*	*0.053*		
13	*5.308*	*0.0055*	*0.0862*	*1.113*	*92.9*	*99.5*	*37.447*	*0.060*		
17	*5.871*	*1.776*	*1.914*	*0.069*	*0.29*	*92.8*	*38.6*	*1.0*		
Mean age ± 2σ			n=3	MSWD=0.06		125.7	±93.0		15.97	0.09

Notes:

Isotopic ratios corrected for blank, radioactive decay, and mass discrimination, not corrected for interfering reactions.

Errors quoted for individual analyses include analytical error only, without interfering reaction or J uncertainties.

Mean age is weighted mean age of Taylor (1982). Mean age error is weighted error of the mean (Taylor, 1982), multiplied by the root of the MSWD where MSWD>1, and also incorporates uncertainty in J factors and irradiation correction uncertainties.

Decay constants and isotopic abundances after Steiger and Jäger (1977).

symbol preceding sample ID denotes analyses excluded from mean age calculations.

Ages calculated relative to FC-2 Fish Canyon Tuff sanidine interlaboratory standard at 28.201 Ma

Decay Constant (LambdaK (total)) = 5.463e-10/a

Correction factors:

$(^{39}Ar/^{37}Ar)_{Ca}$ = 0.0006726 ± 0.000005

$(^{36}Ar/^{37}Ar)_{Ca}$ = 0.00027 ± 0.0000050

$(^{38}Ar/^{39}Ar)_{K}$ = 0.01261

$(^{40}Ar/^{39}Ar)_{K}$ = 0.007439 ± 0.000146

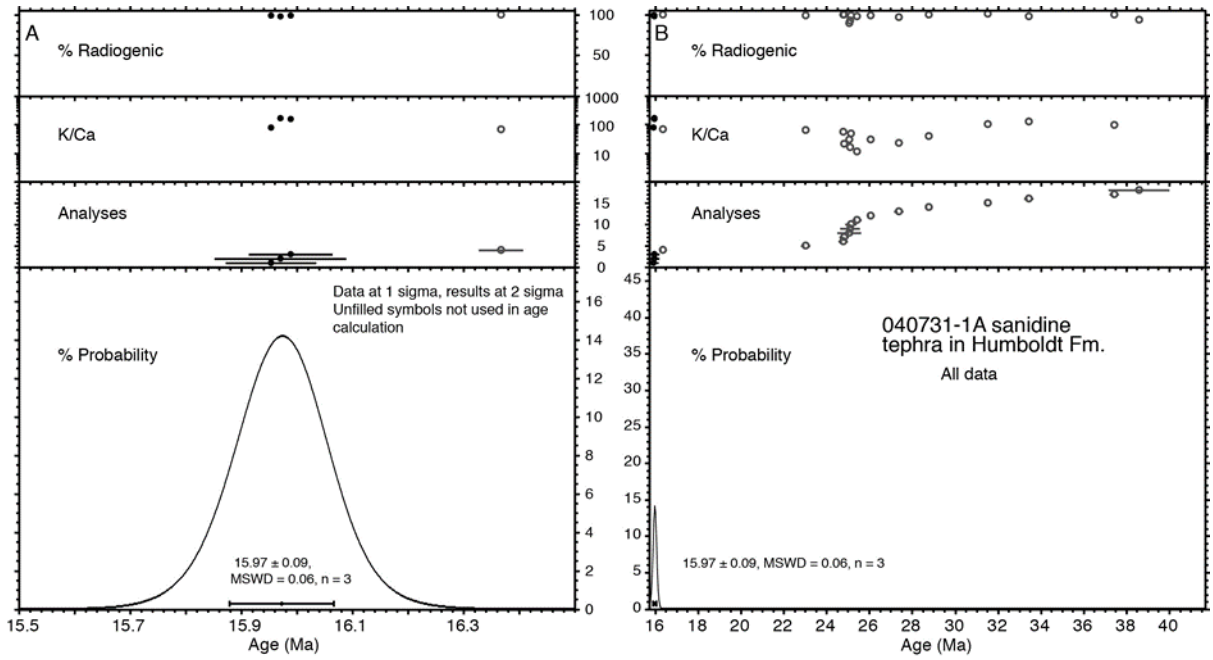

Figure 7. $^{40}Ar/^{39}Ar$ single-crystal, age probability diagrams for sanidine from sample 040731-1A, tephra in Humboldt Formation. A. Diagram showing three youngest grains, which yield a tightly clustered mean of 15.97±0.06 Ma. B. Diagram showing all analyzed grains, which are as old as 38 Ma, which demonstrates some sanidine grains are reworked from older rocks. Depositional age is no older than 15.97±0.06 Ma. Analyses at New Mexico Geochronological Research Laboratory. Unfilled circles not used in age calculations. Dates relative to Fish Canyon Tuff sanidine with an assigned age of 28.201 Ma (Kuiper et al., 2008). MSWD—mean square of weighted deviates.

Inferred Angular Unconformity

Tr Quartz porphyry rhyolite (middle Miocene) Brown to red-brown to deep red or orange red on weathered surfaces, pearly gray to red-brown on fresh surfaces. Locally conspicuously porphyritic with distinctive round, 1–4 mm diameter phenocrysts of quartz as well as feldspar. Locally vesicular with some vesicles filled with quartz, calcite and/or opaline material. The quartz porphyry rhyolite is commonly massive with slabby cleavage locally developed. Inferred to correlate with the similar Willow Creek rhyolite suite, which is extensively exposed in the adjacent Welcome quadrangle, and the Jarbidge Rhyolite, which is widespread throughout northern Elko County (Brueseke et al., 2014; McGrew and Snoke, 2015). It may also correlate with units Tr_1 and Tr_2 in the Heelfly Creek quadrangle in the southwest East Humboldt Range (Dee et al., 2015). Quartz and feldspar-phyric rhyolite porphyry in the Welcome quadrangle yielded an $^{40}Ar/^{39}Ar$ sanidine age of 15.25 ± 0.04 Ma (M.E. Brueseke and W. Hames, unpublished data, personal comm., 2013); similar rhyolites in the Heelfly Creek quadrangle, yielded $^{40}Ar/^{39}Ar$ anorthoclase ages of 15.33 ± 0.01 Ma and 15.37 ± 0.04 Ma (Dee and Henry, unpublished data, personal comm., 2016). Where most prominently exposed at "Red Hill," the quartz porphyry rhyolite could represent a small intrusive plug into Tsu (below) or a small rhyolite dome extruded on top of it. Structural thickness is poorly constrained and probably variable, but ranges up to at least 320 m (500 ft).

Tsu Tertiary sedimentary rocks, undivided (middle to lower Miocene?) Poorly exposed in the north-central part of the quadrangle, this unit probably correlates with Humboldt Formation unit 1 but could also correlate with the sedimentary sequence of Clover Creek, both of which are extensively exposed in the adjacent Welcome quadrangle (McGrew and Snoke, 2015). In the one locality where these rocks crop out they consist of pale cream to pale greenish gray tuffaceous siltstone. The lower contact is fault-bounded, but the exposed structural thickness is approximately 425 m (1400 ft).

Unmetamorphosed Paleozoic Sedimentary Rocks

Mc Chainman Formation (Mississippian) Laminated to very thin-bedded, dark red to pale purple siltstone, pale red to yellowish buff shale, and coarse black sandstone locally containing pebbly or conglomeratic horizons. Localized beds of sedimentary breccia with black chert clasts in a pale lavender matrix resemble the Diamond Peak Formation. Poorly exposed, occurs only on the east side of the southernmost hill in the NE part of the quadrangle. Sparse chert-pebble conglomerate supports correlation with the Chainman Formation rather than the Pilot Shale as originally mapped by Lush (1982). The unit is fault bounded so the exposed thickness of 295 m (970 ft) represents a minimum. A water well located approximately 330 m south of these outcrops penetrates to a depth of 1000 ft (305 m) apparently entirely within the Chainman Formation (Nevada well log 116304).

Mj Joana Limestone (Mississippian) Light gray, bioclastic (crinoidal) limestone overlying the Guilmette Formation forming a single outcrop at the north end of the southernmost hill in the NE part of the quadrangle. The top of the unit is bounded by dark silicified fault breccia, so the exposed thickness of ~92.5 m (300 ft) represents a minimum.

Dg Guilmette Formation (Upper Devonian) Massively bedded to platy, dark gray limestone with abundant calcite veins and widespread brecciation rendering bedding locally difficult to recognize. Commonly fossiliferous, it contains stromatoporoids, bryozoa, corals, crinoid debris, gastropods, and brachiopods (Snelson, 1957; Lush, 1982). The base of the Guilmette Formation is not exposed; the maximum exposed thickness is approximately 430 m (1410 ft).

> **Dg_r Guilmette Formation member (Upper Devonian)** The upper middle part of the Guilmette Formation in the Humboldt Peak quadrangle includes a mappable member, designated as Dg_r, consisting of approximately 42.5 m (140 ft) of pale reddish-gray weathering, very thin-bedded to laminated, silty to sandy micritic limestone. On fresh surfaces this member is extensively burrowed and mottled red and blue-gray to greenish-gray. Locally it contains fossils, including an Atrypid brachiopod.

DSd Dolomite (Devonian to Silurian, undivided) Laminated black, fine- to medium-grained dolomite, thick-bedded medium- to dark-gray dolomite, and quartz sandstone (Lush, 1982). The unit is commonly brecciated and cemented by either a carbonate and/or siliceous matrix between the fragments. The lithologic character of this undivided dolomite unit suggests that it may include some elements of the Silurian Laketown Dolomite but mostly consists of Lower Devonian Sevy Dolomite and Middle Devonian Simonson Dolomite (Lush, 1982). It is fault-bounded, but the structural thickness in Signal Hill is at least 550 m (1800 ft).

Metamorphosed Sedimentary and Igneous Rocks

M€mu Calcite and dolomite marble with calc-silicate paragneiss and metaquartzite (Mississippian to Cambrian, undivided) In most areas this unit probably consists chiefly of Ordovician to Cambrian marble and associated calc-silicate schist, paragneiss, and quartzite. However, in places this unit cannot be reliably separated from overlying dolomitic and calcitic marble units, and so is left undivided. Common rock types include: coarse-grained white marble, medium- to coarse-grained gray marble (locally micaceous), dolomitic marble, coarse-grained cream- to yellow-weathering marble with large blades of tremolite, diopside-bearing white quartzite (probably Kanosh Formation), and thin layers of calcareous paragneiss or calc-schist. Overall, this unit is inferred to correlate with the carbonate-dominated part of the Cordilleran miogeoclinal sequence. Thickness varies dramatically depending on structural position, but on the lower limb of the WLN thickness is locally as little as 150 m (500 ft).

MDgs Graphitic schist and calcareous paragneiss (Mississippian to Upper Devonian?) Graphite-bearing micaceous feldspathic quartzite and quartzofeldspathic schist (commonly calcareous), pelitic schist, and calc-silicate paragneiss, all rich in opaque minerals and weathering to a rusty red brown. Observed only in the WLN, not in the Lizzies Basin gneiss complex. Characteristic metamorphic mineral assemblages in pelitic schist includes: bt + sill ± ky + gt + pl + qz + ilm + hm + ru ± ttn + ap + mnz + zr + gr [+ melt] (McGrew et al., 2000; Hallett and Spear, 2014). Kyanite is observed only on the upper limb of the WLN where it is invariably thickly mantled or completely pseudomorphed by fibrous sillimanite. Invariably migmatitic, the proportion of leucogranitic rock varies from < 25% on the upper limb of the WLN to >67% leucogranite in the hinge zone and on the lower limb. Due to the significant calcareous component of this unit, it is tentatively correlated with the Pilot Shale (Spencer, 1917), but a correlation with the Chainman Formation is also possible. Therefore, the stratigraphically overlying marble units may correlate with the Joana and/or Tripon Pass Limestones (Spencer, 1917; Oversby, 1973). Here, these marble units have been combined with the Mississippian to Cambrian marble unit, undivided. Structural thickness of the graphitic schist varies dramatically depending on structural position; on the lower limb of the WLN it is commonly absent and never more than 5 m (16 ft) thick, but on the upper limb it averages 12–25 m (40–80 ft) thick.

DOdm Dolomitic marble (Devonian to Ordovician, undivided) White to dark gray, medium- to coarse grained typically massive dolomitic marble with subordinate meta-sandstone and calc-silicate rock. Locally includes calcite marble (possibly correlating in part with Upper Devonian Guilmette Formation). The typically massive and relatively homogeneous, predominantly dolomitic character of this unit helps to distinguish it from the more heterogeneous, dominantly calcitic marble of Verdi Peak (O€m) that underlies the Eureka Quartzite. Correlative units include the Ordovician to Silurian Laketown and Fish Haven Dolomites (Richardson, 1913); the Silurian Roberts Mountains Formation (Merriam, 1940); the Devonian to Silurian Lone Mountain Dolomite (Hague, 1883); and the Devonian Sevy and Simonson Dolomites (Nolan, 1930, 1935). In the Pequop Mountains these units have an aggregate thickness of approximately 3300 ft (1000 m) (Camilleri, 2010a), but like other units in the northern EHR, profound plastic attenuation commonly reduces this unit to a structural thickness of less than 36 m (120 ft); in a number of localities it is totally omitted, presumably due to megaboudinage.

Oe Metamorphosed Eureka Quartzite (Ordovician) Coarse-grained, metaquartzite; commonly vitreous gray on fresh fractures, it weathers to white, commonly with dispersed grains of white diopside. Locally it shows gray

streaks due to the presence of sparse, disseminated graphite. It commonly forms a thin, discontinuous layer marking the contact between the marble of Verdi Peak (O€m) and the dolomitic marble (DOdm). It pinches out locally due to tectonic attenuation, but where present is commonly 1–3 m (3–10 ft) thick.

O€m Marble of Verdi Peak (Ordovician to Cambrian, undivided) The marble of Verdi Peak (Cambrian and Ordovician marble of Howard, 1971) consists of pale gray, graphitic, muscovite-bearing calcite ± dolomite marble, calc-silicate marble, and yellow-brown-weathering metadolomite. Characteristic mineral assemblages include: cc ± dol ± pl ± di ± tr ± ep ± gt ± phl ± ttn ± scap (Peters and Wickham, 1994). The unmetamorphosed Ordovician to Upper Cambrian stratigraphy in eastern Elko County defines an aggregate thickness of nearly 4 km (13,000 ft) (McCollum and Miller, 1991). Camilleri (2010a; 2010b) and Thorman (1970) documented a modestly attenuated section 2440 m (8000 ft) thick in the greenschist-facies rocks of the Pequop Mountains and a more intensely attenuated section averaging approximately 550 m (1800 ft) thick in the amphibolite facies terrain of the Wood Hills. Plastic attenuation of these strata reaches an extreme degree in the northern East Humboldt Range. In the Humboldt Peak quadrangle, on the limbs of the WLN the marble of Verdi Peak locally thins to as little as 20–40 m (65–130 ft), less than 1% of its inferred original stratigraphic thickness. In the Lizzies Basin block, thinning appears to be less extreme although assessment of structural thickness is hampered by topographic inaccessibility and by subsequent inflation of the section by younger intrusions; nevertheless, in the western cirque wall of Lizzies Basin it is at least 100–200m (328–656 ft) thick, 2.5–5% of original stratigraphic thickness. Farther south, in the Gordon Creek quadrangle, this unit is still less attenuated and more extensively exposed—attaining structural thicknesses on the order of at least 300–400 m (984–1312 ft)—nearly 10% of original stratigraphic thickness (Sicard, 2012; Sicard and Snoke, in press). Thus the structural attenuation as compared with the unmetamorphosed reference section appears to intensify from south to north across the Humboldt Peak quadrangle from ~10% in the south to ≤ 1–2% farther north.

€Zpm Metamorphosed Prospect Mountain Quartzite (Cambrian to Neoproterozoic protolith age) and McCoy Creek Group (Neoproterozoic protolith age), undivided Micaceous feldspathic quartzite with subordinate pelitic schist, and locally with calc-silicate gneiss and rare para-amphibolite. Commonly migmatitic, with pelitic rocks hosting a higher percentage of leucosome than quartzitic rocks. Leucosome occurs in centimeter-scale to meter-scale concordant pods, sheets, and lenses commonly bordered by bt+sill melanosomes. Characteristic metamorphic mineral assemblages in pelitic schist include: bt + sill + gt +pl + qz + ilm ±ru + ttn + mnz + zr + opq. Thickness varies from approximately 75 m (250 ft) on the lower limb of the WLN near the northwest corner of the quadrangle to a minimum of 245 m (800 ft) near the southwest corner of the quadrangle.

Zmu McCoy Creek Group paragneiss, undivided (Neoproterozoic) Coarse grained micaeous quartzite, feldspathic quartzite, and bt ± sill ± gt schist, locally with subsidiary marble, calc-silicate paragneiss and sparse melanoamphibolite. Contains <67% leucogranitic rock, but intrusions of small-scale leucogranitic bodies are widespread. Due to the difficulty of separating more quartzitic components of this unit from the overlying Prospect Mountain quartzite, the upper contact of this unit was defined at the uppermost marble horizon, thus combining the upper McCoy Creek Group with the Prospect Mountain quartzite. Premo et al. (2014) report U-Pb SHRIMP-RG results on detrital zircons from this sequence showing a strong, Grenville minimum age provenance of 800 to 1250 Ma, supporting correlation with the McCoy Creek Group. Other detrital zircon age peaks in the sequence include 1360–1450, 1600–1880, 2000–2050, and 2600–2940 Ma (Premo et al., 2014). The base of the sequence is unexposed, but the aggregate structural thickness (including the underlying strongly migmatitic phase discussed below) is at least 1000 m (3280 ft).

Zmu_m McCoy Creek Group paragneiss, undivided, migmatitic phase (Neoproterozoic) Severely migmatized McCoy Creek Group paragneiss lithologically similar to undivided McCoy Creek Group paragneiss (Zmu) but containing >67% leucogranitic rock based on visual estimation at outcrop scale. U-Pb SHRIMP-RG geochronology on zircon and monazite indicate episodic crystallization of leucogranite between 100 and 60 Ma, with a subsequent high grade thermal overprint recorded in monazite rims between 40 and 32 Ma (Hallett and Spear, 2015; Premo et al., 2014). The transition from Zmu_m to Zmu occurs gradationally over a short vertical distance of ~60 m (200 ft).

Zmm McCoy Creek Group marble (Neoproterozoic) Discontinuous, coarse grained white marble horizons typically <6 m (20 ft) thick, but ranging up to 120 m in the northeast face of Humboldt Peak. Anomalously high $\delta^{13}C$ values ranging up to 12‰ contrast strongly with the more normal carbon isotope values (0 to -2 ‰) of the inferred Paleozoic marble sequence, strongly supporting correlation with similar high $\delta^{13}C$ McCoy Creek Group marble units in the Pilot and Schell Creek Ranges (Wickham and Peters, 1993). Locally, marble horizons can be traced laterally across the gradational boundary that marks the transition into the Lizzies Basin migmatite complex (Zmu_m above); in such cases the marble units thin dramatically and are progressively replaced by calc-silicate assemblages rich in diopside, grossular garnet and actinolite.

Zms McCoy Creek Group pelitic schist (Neoproterozoic) Coarse grained pelitic schist characterized by the peak assemblage qz + pl + bt + sill + gt + Ksp + ap + mnz + zr + ilm + ru (with rutile and xenotime occurring only as inclusions in garnet) (McGrew et al, 2000;

Hallett and Spear, 2014, 2015). Possibly correlative with McCoy Creek Group unit H (the Osceola Argillite) (Misch and Hazzard, 1962; Miller, 1983). Forms a mappable horizon typically <30 m (100 ft) thick in the upper part of the McCoy Creek paragneiss sequence of Lizzies Basin.

ZXpg Paragneiss of Greys Peak (Neoproterozoic to Paleoproterozoic) Impure micaceous and/or feldspathic metaquartzite and metapsammitic paragneiss, biotite-sillimanite schist (locally with garnet), and rare white metaquartzite or pale to apple green fuchsitic metaquartzite. Also hosts widespread meter-scale layers and boudins of melanocratic amphibolite and garnet amphibolite interpreted as metamorphosed mafic intrusions. Migmatization is widespread with more pelitic components commonly hosting large volumes of leucosome, especially at deeper structural levels on the lower limb of the WLN. Detrital zircon geochronology of most samples defines a strong minimum provenance of Grenville age (800–1250 Ma) supporting correlation with the McCoy Creek Group (Link, 2011; Misch and Hazzard, 1962), but a sample of fuchsitic quartzite shows a much older minimum age provenance of approximately 2400 Ma suggesting that the unit may locally include Paleoproterozoic rocks (Premo et al., 2014 and pers. comm.). Consequently, this unit may correlate in large part with the McCoy Creek Group, but may also include stratigraphically deeper and potentially older rocks.

Intrusive Rocks

Tb Basaltic dikes (middle Miocene) Black, locally amygdaloidal with chilled margins and locally with a diabasic core.

Tgr Biotite granite (lower Miocene to Oligocene?) Medium-grained, equigranular biotite granite forming steeply dipping dikes intruding the southern half of the quadrangle. Resembles the biotite monzogranitic orthogneiss (below) but with little to no foliation and lower color index (<10% biotite). These dikes cut all gneissic units, including the monzogranitic orthogneiss sheets.

Tmg Biotite monzogranite orthogneiss (lower Oligocene to upper Eocene) Weakly to moderately foliated, medium-grained, equigranular biotite monzogranite and subordinate tonalite and granodiorite, locally with small feldspar phenocrysts. At higher structural levels protomylonitic fabrics are well developed and indicate WNW-directed shear. Contains approximately 10% biotite and subequal proportions of oligoclase, alkali feldspar and quartz. Accessory phases include apatite, zircon, monazite, allanite, and opaque phases. Typically forms meter-scale concordant to slightly discordant sheets, but locally forms laccolithic intrusive centers with dimensions on the order of tens of meters. Dated at 29 ± 0.5 Ma by U-Th-Pb zircon and monazite methods (Wright and Snoke, 1993, their sample RM-5).

Tqd Hornblende-biotite quartz dioritic orthogneiss (middle Eocene) Well-foliated (locally with well developed, west-to-northwest-directed protomylonitic fabric at high structural levels), mostly equigranular quartz dioritic orthogneiss consisting of >60% andesine, 15–30% hornblende plus biotite, 10–20% quartz, and sparse to absent alkali feldspar. Titanite is the most abundant accessory mineral, locally forming distinctive coarse amber-colored grains. Other accessories include: apatite, zircon, allanite, epidote, xenotime, scarce garnet, and relatively sparse opaque oxide phases. Forms dark, nearly black-weathering, bold and often jagged outcrops especially prominent in the central part of the range surrounding Lizzies Basin (figs. 2b and 4). There, it forms sills 60–200 m thick extending both southward and especially northward from an intrusive center >500 m thick along the north ridge line of Lizzies Basin. Dated at 40 ± 3 Ma by U-Pb zircon ID-TIMS (Locality A in the map plate) (Wright and Snoke, 1993). Premo et al. (2014) report an overlapping age of 40.9 ± 0.9 Ma (U-Pb zircon SHRIMP) from the cirque east of Humboldt Peak.

TKlg Leucogranite and leucogranitic orthogneiss (Paleogene to Cretaceous) Predominantly moderately to strongly foliated granitic pegmatite, but also including trondhjemitic pegmatite, muscovite-rich two-mica leucogranite, and weakly foliated, late-stage garnet aplite dikes. Foliated leucogranites mostly form small concordant sheets, pods or lenses, commonly bounded by bt + sill melanosomes. In contrast, weakly foliated leucogranitic bodies commonly form dikes cutting gneissic foliation. A folded leucogranitic sheet in the hinge zone of the Winchell Lake fold-nappe yielded a $^{207}Pb^*/^{206}Pb^*$ zircon date of 85 ± 3 Ma (U-Pb locality B in the map plate), resembling leucogranite ages from the southern East Humboldt Range and Ruby Mountains (Snoke et al., 1990; McGrew et al., 2000). More recently, Hallett and Spear (2015) and Premo et al. (2014) have applied U-Pb SHRIMP-RG geochronology to document a history of zircon and monazite crystallization extending from Late Cretaceous to early Paleocene time. Although much of the leucogranite is undoubtedly Late Cretaceous, some leucogranitic rocks are observed cutting or intermingled with the 40 Ma quartz diorite and 29 Ma biotite monzogranitic sheets and therefore must range in age at least into the Oligocene.

ACKNOWLEDGMENTS

The geologic mapping of the East Humboldt Range is a tribute to the mentorship and leadership of Dr. Arthur W. Snoke of the University of Wyoming. In addition, over many years, several undergraduate field assistants contributed significantly to the mapping of the Humboldt Peak quadrangle, most significantly Christopher Jayne and Brian Kirchner (both of Earlham College), and James P. Hogan and Andrew Folfas (from the University of Dayton). In addition, this mapping project profited greatly from discussions and collaborations with Melissa Batum, Calvin Barnes, Phyllis Camilleri, Callum Hetherington, Keith Howard, Michael Hudec, Hugh Hurlow, Karl Mueller, Mark Peters, Karri Sicard, Lawrence Snee, Charles Thorman, Steve Wickham, and numerous other colleagues who have visited the area on field trips. Ben Hallett generously shared access to his results and ideas as his work in the area progressed. I also thank Richard Allmendinger for making the Stereonet 8.0 software package freely available to us as members of the wider academic geological community. Phyllis Ranz at the University of Wyoming contributed greatly through skillful draftsmanship, as did Irene Seelye at the Nevada Bureau of Mines and Geology, who produced the final map.

Funding for this project derived from several sources, including: NSF Research Grants awarded to A.W. Snoke (University of South Carolina and University of Wyoming), University of Wyoming teaching and research fellowships, NSF Post-doctoral Research Fellowship EAR 92-08855 awarded to Allen McGrew, a Geological Society of Nevada quadrangle mapping grant, a grant of financial assistance from Dale Kraemer, and University of Dayton grants in Aid of Research.

Finally, the completion of this project owes much to Christopher Henry of the Nevada Bureau of Mines and Geology, who arranged much-appreciated office and field reviews of this geologic mapping as well as offering a broad array of helpful and insightful advice. In addition to Henry, detailed and insightful office reviews were provided by Joseph Colgan, Seth Dee, Keith Howard, and Charles Thorman.

Research supported in part by the U.S. Geological Survey, National Cooperative Geologic Mapping Program, under USGS STATEMAP award number G16AC00186. The views and conclusions contained in this document are those of the authors and should not be interpreted as necessarily representing the official policies, either expressed or implied, of the U.S. Government.

REFERENCES

Allmendinger, R.W., Cardozo, N.C., and Fisher, D., 2012, Structural geology Algorithms—Vectors & Tensors: Cambridge, England, Cambridge University Press, p. 289.

Brueseke, M., Callicoat, J.S., Hames, W., and Larson, P.B., 2014, Mid-Miocene rhyolite volcanism in northeastern Nevada—the Jarbidge Rhyolite and its relationship to the Cenozoic evolution of the northern Great Basin (USA): Geological Society of America Bulletin, v. 126, p. 1047–1067.

Camilleri, P.A., 2010a, Geologic map of the northern Pequop Mountains, Elko County, Nevada: Nevada Bureau of Mines and Geology Map 171, scale 1:24,000, p. 15.

Camilleri, P.A., 2010b, Geologic map of the Wood Hills, Elko County, Nevada: Nevada Bureau of Mines and Geology Map 172, scale 1:24,000, 1 sheet with text

Camilleri, P.A. and Chamberlain, K.R., 1997, Mesozoic tectonics and metamorphism in the Pequop Mountains and Wood Hills region, northeast Nevada—implications for the architecture and evolution of the Sevier orogen: Geological Society of America Bulletin, v. 109, p. 74–94.

Dallmeyer, R.D., Snoke, A.W., McKee, E.H., 1986, The Mesozoic-Cenozoic tectonothermal evolution of the Ruby Mountains, East Humboldt Range, Nevada—a Cordilleran metamorphic core complex: Tectonics, v. 5, p. 931–954.

Dee, S.M., Dering, G.M., and Henry, C.D., 2015, Preliminary geologic map of the Heelfly Creek quadrangle and adjacent parts of the Tent Mountain, Soldier Peak, and Secret Valley quadrangles, Elko County, Nevada: Nevada Bureau of Mines and Geology Open-File Report 15-4, scale 1:24,000, p. 5.

dePolo, C.M., and LaPointe, D.D., editors, 2011, The 21 February 2008 M_w 6.0 Wells, Nevada earthquake—a compendium of earthquake-related investigations prepared by the University of Nevada, Reno (paper version, includes links to appendices which are only available online): Nevada Bureau of Mines and Geology Special Publication 36, 507 p.

Dohrenwend, J.C., Schell, B.A., Moring, B.C., 1991a, Reconnaissance photogeologic Map of Young Faults in the Elko 1 by 2 degree quadrangle, Nevada and Utah: U.S. Geological Survey, Miscellaneous Field Studies Map MF-2179 1 sheet, scale 1:250,000.

Dohrenwend, J.C., McKittrick, M.A., and Moring, B.C., 1991b, Reconnaissance photogeologic map of young faults in the Wells 1° by 2° quadrangle, Nevada, Utah, and Idaho: U.S. Geological Survey Miscellaneous Field Studies Map MF-2184, 1 sheet, scale 1:250,000.

Drew, J., 2013, Cretaceous and Eocene U-Pb zircon migmatite ages from the East Humboldt Range metamorphic core complex, Nevada, University of Nevada, Las Vegas, M.S. thesis, p. 65.

Hague, A., 1883, Report on the geology of the Eureka district, Nevada: U.S. Geologic Survey, 3rd Annual Report, v. 37, p. 237–272.

Haines, S.H., and van der Pluijm, B.A., 2010, Dating the detachment fault system of the Ruby Mountains, Nevada—significance for the kinematics of low-angle normal faults: Tectonics, v. 29, TC4028, doi:10.1029/2009TC002552.

Hallet, B.W. and Spear, F.S., 2014, The P-T history of anatectic pelites of the northern East Humboldt Range, Nevada—evidence for Tectonic loading, decompression, and anataxis: Journal of Petrology, v. 55, no. 1, p. 3–36.

Hallet, B.W., and Spear, F.S., 2015, Monazite, zircon, and garnet growth in migmatitic pelites as a record of metamorphism and partial melting in the East Humboldt Range, Nevada, American Mineralogist, v. 100, p. 951–972.

Henry, C.D., and Colgan, J.P., 2011, The regional structural setting of the 2008 Wells earthquake and Town Creek Flat

Basin—implications for the Wells earthquake fault and adjacent structures: Nevada Bureau of Mines and Geology Special Publication 36, p. 53–64.

Howard, K.A., 1971, Paleozoic metasediments in the northern Ruby Mountains, Nevada: Geological Society of America Bulletin, v. 82, p. 259–264.

Howard, K.A., 1980, Metamorphic infrastructure in the northern Ruby Mountains, Nevada, *in* Crittenden, M.D., Jr., Coney, P.J., and Davis, G.H., editors, Cordilleran Metamorphic Core Complexes: Geological Society of America Memoir 153, p. 335–347.

Hurlow, H.A., 1987, Structural geometry, fabric, and chronology of a Tertiary extensional shear zone-detachment system, southwestern East Humboldt Range, Elko County, Nevada: Laramie, University of Wyoming, M.S. thesis, p. 141.

Hurlow, H.A., Snoke, A.W., and Hodges, K.V., 1991, Temperature and pressure of mylonitization in a Tertiary extensional shear zone, Ruby Mountains-East Humboldt Range, Nevada—tectonic implications: Geology, v. 19, p. 82–86.

King, C., 1878, Systematic geology—geological exploration of the Fortieth Parallel, v. 1: Washington, D.C., U.S. Government Printing Office, 803 p.

Kistler, R.W., Ghent, E.D., and O'Neil, J.R., 1981, Petrogenesis of garnet two-mica granites in the Ruby Mountains, Nevada: Journal of Geophysical Research, v. 86, p. 10,591–10,606.

Kuiper, K.F., Deino, A., Hilgen, F.J., Krijgsman, W., Renne, P.R., and Wijbrans, J.R., 2008, Synchronizing rock clocks of Earth history: Science, v. 320, p. 500–504.

Link, P.K., 2011, Systematic regional patterns in detrital-zircon populations from Cryogenian, Ediacaran and Cambrian sandstones, Brigham Group and Tintic Quartzite, northern Utah thrust belt: Geological Society of America Abstracts with Programs, v. 43, 56 p.

Lush, A.P., 1982, Geology of part of the northern East Humboldt Range, Elko County, Nevada: Columbia, University of South Carolina, M.S. thesis, 138 p.

Lush, A.P., McGrew, A.J., Snoke, A.W., and Wright, J.E., 1988, Allochthonous Archean basement in the north East Humboldt Range, Nevada: Geology, v. 16, p. 349–353.

MacCready, T.M., 1996, Misalignment of quartz c-axis fabrics and lineations due to oblique final strain increments in the Ruby Mountains core complex, Nevada: Journal of Structural Geology, v. 18, No. 6, p. 765–776.

MacCready, T.M., A.W. Snoke, J.E. Wright and K.A. Howard, 1997, Mid-crustal flow during Tertiary extension in the Ruby Mountains core complex, Nevada: GSA Bulletin; December 1997; v. 109; no. 12; p. 1576–1594.

McCollum, L.B., and Miller, D. M., 1991, Cambrian stratigraphy of the Wendover area, Utah and Nevada: U. S. Geological Survey Bulletin 1948, 43 p.

McGrew, A.J., 1992, Tectonic evolution of the northern East Humboldt Range, Elko County, Nevada: Laramie, University of Wyoming, Ph.D. dissertation, p. 191.

McGrew, A.J., and Casey, M., 1998, Quartzite fabric transition in a Cordilleran metamorphic core complex, *in* Snoke, A. W., Tullis, J., and Todd, V.R., editors, Fault-related rocks—A photographic atlas: Princeton, N.J., Princeton University Press, p. 484–489.

McGrew, A.J., Peters, M.T., and Wright, J.E., 2000, Thermobarometric constraints on the tectonothermal evolution of the East Humboldt Range metamorphic core complex, Nevada: Geological Society of America Bulletin, v. 112, p. 45–60.

McGrew, A.J., and Premo, W.R., 2011, The Angel Lake gneiss complex of northeastern Nevada and the southwestern limits of Archean to Paleoproterozoic basement in North America: Geological Society of America Abstracts with Programs, v. 43, no. 5, 435 p.

McGrew, A.J., and Snee, L.W., 1994, $^{40}Ar/^{39}Ar$ thermochronologic constraints on the tectonothermal evolution of the northern East Humboldt Range metamorphic core complex, Nevada: Tectonophysics, v. 238, p. 425–450.

McGrew, A.J., and Snoke, A.W., 2010, SHRIMP-RG U-Pb isotopic systematics of zircon from the Angel Lake orthogneiss, East Humboldt Range, Nevada—is this really Archean crust?: Geosphere, v. 6, no. 6, p. 962–965, doi: 10.1130/GES00526.1.

McGrew, A.J., and Snoke, A.W., 2015, Geologic map of the Welcome and adjacent part of the Wells quadrangle, Elko County, Nevada, Nevada Bureau of Mines and Geology, Map 184 scale 1:24,000, inset 1:12,000, p. 40.

Merriam, C.W., 1940, Devonian stratigraphy and paleontology of the Roberts Mountains region, Nevada: Geological Society of America Special Paper 25, 114 p.

Miller, D.M., 1983, Allochthonous quartzite sequence in the Albion Mountains, Idaho, and proposed Proterozoic Z and Cambrian correlatives in the Pilot Range, Utah and Nevada, *in* Miller, D. M., Todd, V.R., and Howard, K.A., editors, Tectonics and stratigraphic studies in the eastern Great Basin: Geological Society of America Memoir 157, p. 191–213.

Misch, P., and Hazzard, J.C., 1962, Stratigraphy and metamorphism of late Precambrian rocks in central northeastern Nevada and adjacent Utah: American Association of Petroleum Geologists Bulletin, v. 46, p. 289–343.

Mueller, K.J., 1992, Tertiary basin development and exhumation of the northern East Humboldt Range–Wood Hills metamorphic complex, Elko County, Nevada: University of Wyoming, Laramie, Ph.D. dissertation, 205 p.

Munroe, J.S., and Laabs, B.J.C., 2011, New investigations of pleistocene glacial and pluvial records in ortheastern Nevada, *in* Lee, J., and Evans, J. P., editors, Geologic field trips to the Basin and Range, Rocky Mountains, Snake River plain, and terranes of the U.S. Cordillera: Geological Society of America Field Trip Guide 21, p. 1–25.

Munroe, J.S., and Laabs, B.J.C., 2013, Temporal correspondence between pluvial lake highstands in the southwestern US and Heinrich Event 1: Journal of Quaternary Science, v. 28, p. 49–58.

Nolan, T.B., 1930, Paleozoic formations in the Gold Hill quadrangle, Utah: Washington Academy of Sciences Journal, v. 20, p. 421–432.

Nolan, T.B., 1935, The Gold Hill mining district, Utah: U.S. Geologic Survey Proffesional Paper 177, 172 p.

Osborn, G., and Bevis, K., 2001, Glaciation in the Great Basin of the western United States: Quaternary Science Reviews, v. 20, p. 1377–1410.

Oversby, B.S., 1973, New Mississippian formation in northeastern Nevada and its possible significance: American Association of Petroleum Geologists, v. 57, no. 9, p. 1779–1783.

Peters, M.T., and Wickham, S.M., 1994, Petrology of upper amphibolite facies marbles from the East Humboldt Range, Nevada, USA—evidence for high-temperature, retrograde,

hydrous volatile fluxes at mid-crustal levels: Journal of Petrology, v. 35, p. 205–238.

Premo, W.R., Castiñeiras, P., and Wooden, J.L., 2008, SHRIMP-RG U-Pb isotopic systematics of zircon from the Angel Lake orthogneiss, East Humboldt Range, Nevada—is this really Archean crust?: Geosphere, v. 4, no. 6, p. 963–975.

Premo, W.R., Castiñeiras, P., and Wooden, J.L., 2010, SHRIMP-RG U-Pb isotopic systematics of zircon from the Angel Lake orthogneiss, East Humboldt Range, Nevada—is this really Archean crust?: REPLY: Geosphere, v. 6, no. 6, p. 966–972, doi: 10.1130/GES00592.1.

Premo, W.R., Moscati, R.J., McGrew, A.J., and Snoke, A.W., 2014, New U-Pb zircon geochronology of Precambrian paragneisses and late Phanerozoic orthogneisses of the Angel Lake-Lizzie Basin region of the East Humboldt Range, northeastern Nevada—a comparison with the thermal chronology at Lamoille Canyon in the adjacent Ruby Mountains: Geological Society of America Abstracts with Programs, v. 46, p. 33.

Reheis, M.C., Sarna-Wojcicki, A., Reynolds, R.L., Repenning, C.A., and Mifflin, M.D., 2002, Pliocene to middle Pleistocene lakes in the western Great Basin: Ages and connections, *in* Hershler, R., Madsen, D.B., and Currey, D.R., editors, Great Basin aquatic systems history: Washington, D.C., Smithsonian Institution Press, Smithsonian Contributions to the Earth Sciences, no. 33, p. 53–108.

Richardson, G. B., 1913, The Paleozoic section in northern Utah: American Journal of Science, v. 36, p. 406–413.

Sharp, R.P., 1938, Pleistocene glaciation in the Ruby-East Humboldt Range, northeastern Nevada: Journal of Geomorphology, v. 1, no. 4, p. 296–323.

Sharp, R.P., 1939, Basin-Range structure of the Ruby-East Humboldt Range, northeastern Nevada: Geological Society of America Bulletin, v. 50, p. 881–920.

Sharp. R.P., 1940, Geomorphology of the Ruby-East Humboldt Range, Nevada: Geological Society of America Bulletin, v. 51, p. 337–372.

Sicard, K.R., 2012, The relationship between Cretaceous and Tertiary magmatism and structural development in the southeastern East Humboldt Range, part of the Ruby-East Humboldt core complex, northeast Nevada: Laramie, University of Wyoming, M.S. thesis, 138 p.

Sicard, K.R., and Snoke, A.W., in press, Geologic map of the Gordon Creek quadrangle, Elko County, Nevada, Nevada Bureau of Mines and Geology, scale 1:24,000.

Snelson, S., 1957, The geology of the northern Ruby Mountains and the East Humboldt Range, Elko County, Nevada: Seattle, University of Washington, Ph.D. dissertation, 214 p.

Snoke, A.W., 1980, Transition from infrastructure to suprastructure in the northern Ruby Mountains, Nevada, *in* Crittenden, M.D., Jr., Coney, P.J., and Davis, G.H., editors, Cordilleran metamorphic core complexes: Boulder, Colorado, Geological Society of America Memoir 153, p. 287–333.

Snoke, A. W., and Miller, D. M., 1988, Metamorphic and tectonic history of the northeastern Great Basin, *in* Ernst, W. G., editor, Rubey Volume No. VII, Metamorphism and crustal evolution of the western United States: Prentice-Hall, p. 606–648.

Snoke, A.W., McGrew, A.J., Valasek, P.A., and Smithson, S.B., 1990, A crustal cross section for a terrain of superimposed shortening and extension—Ruby Mountains-East Humboldt Range metamorphic core complex, Nevada, *in* Salisbury, M.H., and Fountain, D.M., editors, Exposed cross sections of the continental crust: Dordrecht, The Netherlands, Kluwer Academic Publishers, p. 103–135.

Snoke, A.W., Howard, K.A., McGrew, A.J., Burton, B.R., Barnes, C.G., Peters, M.T., and Wright, J.E., 1997, The grand tour of the Ruby–East Humboldt metamorphic core complex, northeastern Nevada: Part 1—introduction & road log, *in* Link, P.K., and Kowallis, B.J., editors, Proterozoic to recent stratigraphy, tectonics, and volcanology, Utah, Nevada, southern Idaho and central Mexico: Provo, Utah, Brigham Young University Geology Studies, v. 42, Part 1, p. 225–269.

Spencer, A.C., 1917, The geology and ore deposits of Ely, Nevada: U.S. Geological Survey Professional Paper 96, 189 p.

Steiger, R.H., and Jager, E., 1977, Subcommission on geochronology: Convention on the use of decay constants in geo- and cosmochronology, Earth Planet: Science Letter 36, . 359–362.

Sullivan, W.A., and Snoke, A.W., 2007, Comparative anatomy of core-complex development in the northeastern Great Basin, U.S.A.: Rocky Mountain Geology, v. 42, p. 1–29.

Taylor, S.R., 1982, Planetary science; a lunar perspective. Lunar and Planetary Institute, Houston.

Thorman, C.H., 1970. Metamorphosed and nonmetamorphosed Paleozoic rocks in the Wood Hills and Pequop Mountains, northeast Nevada: Geological Society of America Bulletin, v. 81, p. 2417–2448.

Thorman, C.H., and Brooks, W.E., 2011, Bedrock geology of the ranges bounding the Wells earthquake of February 21, 2008: Nevada Bureau of Mines and Geology Special Publications 36, p. 65–78.

Wayne, W.J., 1984, Glacial chronology of the Ruby Mountains–East Humboldt Range, Nevada: Quaternary Research, v. 21, p. 286–303.

Wickham, S. M., and Peters, M. T., 1993, High $\delta^{13}C$ Neoproterozoic carbonate rocks in western North America: Geology, v. 21, p. 165–168.

Wright, J.E., and Snoke, A.W., 1993, Tertiary magmatism and mylonitization in the Ruby-East Humboldt metamorphic core complex, northeastern Nevada—U-Pb geochronology and Sr, Nd, Pb isotope geochemistry: Geological Society of America Bulletin, v. 105, p. 935–952.

Suggested Citation:

McGrew, A., 2018, Geologic map of the Humboldt Peak quadrangle, Elko County, Nevada: Nevada Bureau of Mines and Geology Map 186, scale 1:24,000, 23 p.